Hydrogen Production via a High-Efficiency Low-Temperature Steam Reformer

Final Report
For the period September 30, 2004 to September 30, 2005

Paul K. T. Liu
Project Director
(412) 826-3711

November 11, 2005

PREPARED FOR THE UNITED STATES
DEPARTMENT OF ENERGY
Under Cooperative Agreement
No. DE-FG36-04GO14330

By
MEDIA AND PROCESS TECHNOLOGY, INC.
1155 William Pitt Way
Pittsburgh, PA 15238

EXECUTIVE SUMMARY

Fuel cells are promoted by the US government as a viable alternative for clean and efficient energy generation. It is anticipated that the fuel cell market will rise if the key technical barriers can be overcome. One of them is certainly fuel processing and purification. Existing fuel reforming processes are energy intensive, extremely complicated and capital intensive; these disadvantages handicap the scale-down of existing reforming process, targeting distributed or on-board/stationary hydrogen production applications. Our project involves the bench-scale demonstration of a high-efficiency low-temperature steam reforming process. Hydrogen production can be operated at 350 to 400ºC with our invention, as opposed to >800ºC of existing reforming. In addition, our proposed process improves the start-up deficiency of conventional reforming due to its low temperature operation.

The objective of this project is to demonstrate the invented process concept via a bench scale unit and verify mathematical simulation for future process optimization study. Under this project, we have performed the experimental work to determine the adsorption isotherm, reaction kinetics, and membrane permeances required to perform the process simulation based upon the mathematical model developed by us. A ceramic membrane coated with palladium thin film fabricated by us was employed in this study. The adsorption isotherm for a selected hydrotalcite adsorbent was determined experimentally. Further, the capacity loss under cyclic adsorption/desorption was confirmed to be negligible. Finally a commercial steam reforming catalyst was used to produce the reaction kinetic parameters required for the proposed operating condition. With these input parameters, a mathematical simulation was performed to predict the performance of the invented process. According to our simulation, our invented hybrid process can deliver 35 to 55% methane conversion, in comparison with the 12 and 18-21% conversion of the packed bed and an adsorptive reactor respectively. In addition CO contamination with <10 to 120 ppm is predicted for the invented process depending upon the cycle time for the PSA type operation. In comparison, the adsorption reactor can also deliver a similar CO contaminant at the low end; however, its high end reaches as high as 300 ppm based upon the simulation of our proposed operating condition. Our experimental results for the packed bed and the membrane reactor deliver 12 and 18% conversion at 400°C, approaching the conversion by the mathematical simulation. Due to the time constraint, the experimental study on the conversion of the invented process has not been complete. However, our in-house study using a similar process concept for the water gas shift reaction has demonstrated the reliability of our mathematical simulation for the invented process. In summary, we are confident that the invented process can deliver efficiently high purity hydrogen at a low temperature (~400°C).

According to our projection, the invented process can further achieve 5% energy savings and ~50% capital savings over conventional reforming for fuel cell applications. The pollution abatement potential associated with the implementation of fuel cells, including the elimination of nitrogen oxides and CO, and the reduction in volatile organics and CO_2, can thus be realized with the implementation of this invented process. The projected total market size for equipment sale for the proposed process in US is $1.5 billion annually.

Table of Contents

List of Figures

List of Tables

1. Introduction

Transportation accounts for 2/3 of the 20 million barrels of oil consumed each day in the US. The US currently imports 55% of the petroleum used. In response to the energy security concerns posed by reliance on foreign sources, as well as concerns about regional air pollution and greenhouse gas emissions, the U.S. DOE has initiated a number of programs to develop technologies that offer improved energy efficiency and that produce and utilize energy from diverse domestic and renewable sources. In the 2003 State of the Union Address, President Bush reaffirmed the Nation's commitment to energy independence and an improved environment by proposing $1.2 billion in research funding for hydrogen and fuel cell technologies over the next five years. Subsequently, the President proposed a Hydrogen Fuel Initiative that complements FreedomCAR to develop both a hydrogen infrastructure for the low-cost production of hydrogen and advanced hydrogen fuel cell vehicles. Our invented process offers an energy efficient and economically attractive solution to produce hydrogen for these target applications.

2. Technical Summary

Our project involves the bench-scale demonstration of a high-efficiency low-temperature steam reforming process. Hydrogen production can be operated at 350 to 400ºC with our invention, as opposed to >800ºC of existing reforming. We have performed the experimental work to determine the adsorption isotherm, reaction kinetics, and membrane permeances required to perform the process simulation based upon the mathematical model developed by us. Ceramic Membrane deposited with Pd thin prepared by us was found suitable for proposed application environment. In addition, its permeance and selectivity were found adequate for the invented process. Its permeance for hydrogen at 450C is about 10 $m^3/m^2/hr/bar^{0.5}$. The selectivity is about 100 for hydrogen over CO, CO_2, and N_2 (a substitute for methane) based upon the single component permeance measurement. The permeances for CO, CO_2 and N_2 are believed to be resulted from defects of the membrane/leaks of the module because Knudsen diffusion trends were followed for these components. Hydrotalcite prepared by us was found adequate for the adsorption of CO_2 for the invented process. The adsorption isotherm for the selected hydrotalcite adsorbent was determined experimentally at 400 and 450°C and up to 6 bar. The capacity in the neighborhood of 0.3 mmol/g at 1 bar and >4 mmol/g at 6 bar. A Freundlich adsorption isotherm was applied to describe well the CO_2 uptake vs pressure. Further, the capacity loss under cyclic adsorption/desorption was confirmed very insignificant, i.e., <5% loss after the 1st cycle and negligible for >1st cycle. Finally a commercial steam reforming catalyst was used to generate the reaction kinetic parameters required for the proposed operating condition at 350 and 400°C. Although the reaction temperature is low and no literature data is available, we were able to reach the thermodynamic conversion in a packed bed under the proposed operating condition. This implies that the reaction kinetics with the commercial catalyst at this extremely low temperature is adequate for the invented process. The parameters obtained experimentally were used for the mathematical simulation of the proposed process.

According to our simulation with the input parameters obtained experimentally above, our invented hybrid process can deliver 35 to 55% methane conversion, in comparison with the 12 and 18-21% conversion of the packed bed and an adsorptive reactor respectively. In addition CO contamination with <10 to 120 ppm is predicted for the invented process depending upon the

cycle time for the PSA type operation. In comparison, the adsorption reactor can also deliver a similar CO contaminant at the low end; however, its CO contamination at the high end reaches as high as 300 ppm based upon the simulation of our proposed operating condition. Our experimental results for the packed bed and the membrane reactor deliver 12 and 18% conversion respectively at 400°C, approaching the conversion by the mathematical simulation. Due to the time constraint, the experimental study on the conversion of the invented process has not been complete. However, our in-house study using a similar process concept for the water gas shift reaction has demonstrated the reliability of our mathematical simulation for the invented process. In summary, we are confident that the invented process can deliver efficiently high purity hydrogen at a low temperature (~400°C).

According to our projection, the invented process can achieve 5% energy savings and ~50% capital savings over conventional reforming for fuel cell applications. The pollution abatement potential associated with the implementation of fuel cells, including the elimination of nitrogen oxides and CO, and the reduction in volatile organics and CO_2, can thus be realized with the implementation of this invented process.

3. Description of Invented Process

Our project involves the bench-scale demonstration of an innovative process concept: a high-efficiency, low-temperature reactor for steam reforming, targeting distributed/stationary/on-board hydrogen production. Hydrogen production can be operated at 350 to 400ºC with our invention, as opposed to >800ºC of existing reforming. Existing processes are (i) energy intensive due to the requirement of steam (as a reactant) supply at this high temperature, (ii) complicated due to the requirement of water-gas-shift reaction and CO-polishing post reforming, and (iii) capital intensive due to the requirement of special metallurgical alloys for this harsh operating condition. These disadvantages handicap the scale-down of existing reforming process for distributed or on-board/stationary hydrogen production applications. The essence of our proposed process is the employment of a unique adsorption (A)- and membrane (M)-enhanced reformer developed by us (see process scheme below), which can preferentially allow H_2 permeation and CO_2 adsorption simultaneously, the two final reaction products from steam reforming. Thus, the reformer can produce hydrogen product continuously until the adsorbent is saturated for regeneration via pressure swing (PSA). This unique reactor configuration, having only one product stream, can be viewed as a simplified, but upgraded, membrane reactor (MR) under pressure swing operation, suitable for scaled-down steam reforming process. MR and AR proposed in the literature allow only one of the reaction products, such as hydrogen, or CO_2, removal; their reaction rate is not enhanced sufficiently to achieve significant reforming at this low temperature as discussed in Sec. 5.

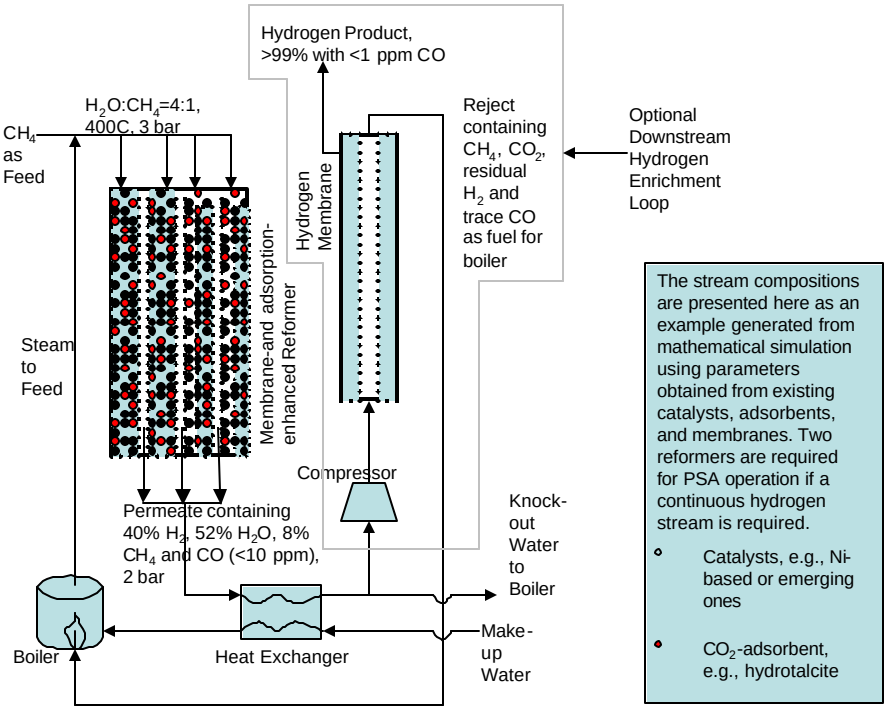

Hydrogen Production via Steam Reforming with Membrane- and Adsorption-Enhanced Reactor at Low Temperature (350 to 400C)

According to our simulation, hydrocarbon conversion with this proposed process concept could be quadrupled over the thermodynamic conversion level; thus, efficient reforming can be accomplished at this low temperature range (see Sec. 5 for details). The hydrogen product stream with ~92% purity (balance is CH_4) is ready as feedstock for fuel cell applications. This product, if desired, can be further enriched to >99% hydrogen with <1 ppm CO with a down stream hydrogen separator using the same type of the hydrogen selective membrane as indicated in the above process scheme.

4. Benchmarking with Existing and Emerging Processes

❑ *Comparison with Existing Steam Methane Reforming*

The key reactions of the steam methane reforming (SMR) process are listed below:

$CH_4 + H_2O = CO + 3H_2$	$?H_{298}$ = 206 kJ/mol	Eq. 1
$CH_4 + 2H_2O = CO_2 + 4\ H_2$	$?H_{298}$ = 165 kJ/mol	Eq. 2
$CO + H_2O = CO_2 + H_2$	$?H_{298}$ = -41 kJ/mol	Eq. 3

Eq. 1 and 2 are highly exothermic. Their forward reactions are favored by high temperature. The water-gas shift reaction, eq. 3, is moderately endothermic, favored by low temperature. To produce a hydrogen stream efficiently (favored by high temperature) with a low level of CO (favored by low temperature) for fuel cell applications, evidently a dilemma exists with existing SMR process. Existing industrial

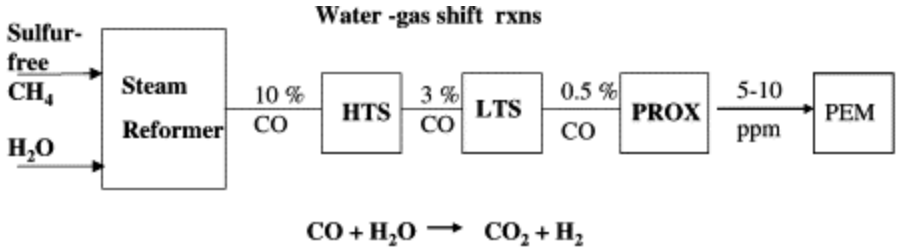

Hydrogen production via SMR is generally operated at 800 to 900ºC to achieve a high level of conversion, ~70% using H_2O/CH_4 4 to 6. In addition to the high temperature, post treatment including WGS, hydrogen separator and CO polishing are required to meet fuel cell spec as described in the process scheme above.

In comparison, our proposed reformer can reduce the reaction temperature to =400ºC, without sacrificing the CH_4 conversion. Our proposed process offers the advantages below:

- No water-gas-shift (WGS) reactor is required. WGS is integrated in our proposed SMR reactor.
- No post treatment for CO clean-up is necessary. CO level is expected to meet the spec with the low temperature reforming and H_2 & CO_2 removal in-situ.
- All heating and cooling requirements involve the temperature range of up to 400 vs >800ºC of existing reforming.
- The low reactor temperature, = 400ºC, offers a tremendous advantage (as opposed to the 800ºC of existing's) with regard to quick start-up required for the mobile application [9].
- The process is ultra-compact, comprising of simplified membrane reactors, one heat exchanger, and one steam generator/boiler. Down stream hydrogen enrichment, if desired, can be achieved by a simplified treatment train comprising one membrane separator using the same type of the hydrogen selective membrane, and one compressor.

Finally, to overcome the heat supply at >>800ºC required by conventional SMR, a modified version, autothermal reforming (ATR) combining partial oxidation and steam reforming, has been actively pursued for the mobile application due to its improvement in start-up. However, ATR is intrinsically energy inefficient and is complex to design and operate. Our proposed process improves the start-up deficiency of conventional reforming due its low temperature operation while enhancing the energy efficiency and capital cost of the conventional reforming.

Two emerging technologies have been actively pursued presently to improve the SMR process for distributed/on-board hydrogen production. They are discussed below:

- **Comparison with Emerging Technology: Adsorptive Reactor for SMR**

Incorporating a selective CO_2 adsorbent in a conventional packed bed SMR reactor (i.e., using a mixed bed of the catalyst and the adsorbent), the conversion of CH_4 to CO_2 through Eq. 2 is favored, as is the production of CO_2 through CO intermediate via Eq. 3. According to the literature, this adsorptive reactor (AR) operated at a moderate temperature of 450ºC allows direct production of ~90% hydrogen (at ~60-70% conversion) from the reactor at the reactor pressure. The impurities in the hydrogen product consist primarily of methane (<10 mol%) and trace

quantities (<50 ppm level) of carbon oxides. The chemisorption is periodically regenerated by PSA operation. In comparison, ~25% conversion is delivered in a conventional SMR reactor under this operating condition. Although the improvement via the CO_2 removal in an AR is significant, an extremely high degree of CO_2 removal is required. According to the calculation using a batch SMR reactor, ~99.7% CO_2 removal is required in order to deliver the stream with the above quality. As a result, the operation time of the AR has to be shortened to keep the effluent concentration of CO at a low level. Thus, the hydrogen productivity from AR is low; the fraction of unused bed for adsorption is extremely high, e.g., 0.8 as described in Ref. 5. In summary, the AR concept is sound in reducing the reaction temperature (down to 450 - 500ºC) and delivering a purer hydrogen product stream via in-situ CO_2 removal. However, to keep the CO contaminant level low hydrogen productivity must be sacrificed due to the under utilization of the adsorptive reactor bed.

- **Comparison with Emerging Technology: Membrane Reactor (MR) for SMR**

The benefit of the membrane reactor (MR) technology has been established for a wide range of industrially significant processes as detailed in the book entitled Catalytic Membrane Reactor co-authored by our co-inventor, Prof. Theo T. Tsotsis. Instead of the CO_2 removal in AR, most MR's remove hydrogen to overcome conversion limitation imposed by thermodynamics. In the case of SMR, the methane conversion theoretically can reach 100% with a perfect membrane, i.e., infinite selectivity for hydrogen over others, is available. In practice, however, such an ideal situation cannot be accomplished even using a perfect membrane due to the reasons below:

- The benefit from the in-situ removal of hydrogen by the membrane declines (along the length of the tubular reactor) once the conversion reaches a significant level. The accumulation of the other reaction product, CO_2 dilutes the benefit achieved by the hydrogen removal, according to the equilibrium relationship, e.g., $K_{eq} = [CO_2][H_2]/[CO][H_2O]$ for WGS. Thus, the forward reactions of Eq. 1 to 3 will continue but at a much slower rate, which become impractical eventually.
- The partial pressure of hydrogen in the MR, which determines the permeation rate of hydrogen, is diluted significantly when CO_2 accumulates in the reactor. Thus hydrogen removal becomes very inefficient.

The above two factors explain the limited benefit of the SMR-MR. Our simulation presents a side-by-side comparison for the MR and our proposed reactor using our selected membrane at the target operating temperature, 400ºC. ~30% conversion can be achieved with the MR which is double of the conversion achieved by the conventional packed bed. With the additional removal of CO_2 via our proposed reactor concept, the methane conversion reaches ~70%, comparable to the conversion level of existing industrial process using a packed bed at 800 to 900ºC. In addition, hydrogen recovery is ~100% because no reject is required under our proposed reactor configuration, as opposed to ~80% in a typical MR due to the loss of hydrogen in the reject, which cannot be removed economically. Finally the CO contaminant level in the proposed reactor is one order-of-magnitude less than that in the MR using the selectivity of our selected membrane (~50 for H_2/CO). Again, the build-up of CO_2 in the typical MR does not drive the conversion of CO sufficiently to keep CO near the negligible level.

5. Mathematical Simulation of Invented Process

A mathematical model was developed to describe the proposed hybrid reactor previously, which is attached in Appendix for reference. Some modifications have been made under this project to reflect the adsorbent, membrane and catalyst properties experimentally obtained in Sec. 6. The mathematical simulation has been performed based upon the thermodynamic and rate parameters obtained from Sec. 6, and the physical parameters of the reactors summarized below:

Feed Composition: CH_4:H_2O:H_2 1:4:0.1
Temperature: 400 °C
Pressure:
Feed Side 4 atm,
Permeate Side: 1 atm
Membrane Properties
N_2 = 0.0699*1.553e-6
H_2 = 5.3466*1.553e-6
CH_4 = (28/16) ^0.5*N_2
H_2O = (28/18) ^0.5*N_2
CO = 0.0683*1.553e-6
CO_2 = 0.0551*1.553e-6
Catalyst & Adsorbent
Catalyst weight: 30 gm
Adsorbent weight: 70 gm
Sweep Ratio = 0.1 * (total feed side flow rate)

The simulation results for the packed bed and the membrane reactor is presented Figure 1 and Figure 2. According to our simulation with the input parameters obtained experimentally above, our invented hybrid process can deliver 35 to 55% methane conversion, in comparison with the 12 and 18-21% conversion of the packed bed and an adsorptive reactor respectively. In addition CO contamination with <10 to 120 ppm is predicted for the invented process depending upon the cycle time for the PSA type operation. In comparison, the adsorption reactor can also deliver a similar CO contaminant at the low end; however, its CO contamination at the high end reaches as high as 300 ppm based upon the simulation of our proposed operating condition. Our experimental results for the packed bed and the membrane reactor deliver 12 and 18% conversion respectively at 400°C, approaching the conversion by the mathematical simulation. Due to the time constraint, the experimental study on the conversion of the invented process has not been complete. However, our in-house study using a similar process concept for the water gas shift reaction has demonstrated the reliability of our mathematical simulation for the invented process. In summary, we are confident that the invented process can deliver efficiently high purity hydrogen at a low temperature (~400°C).

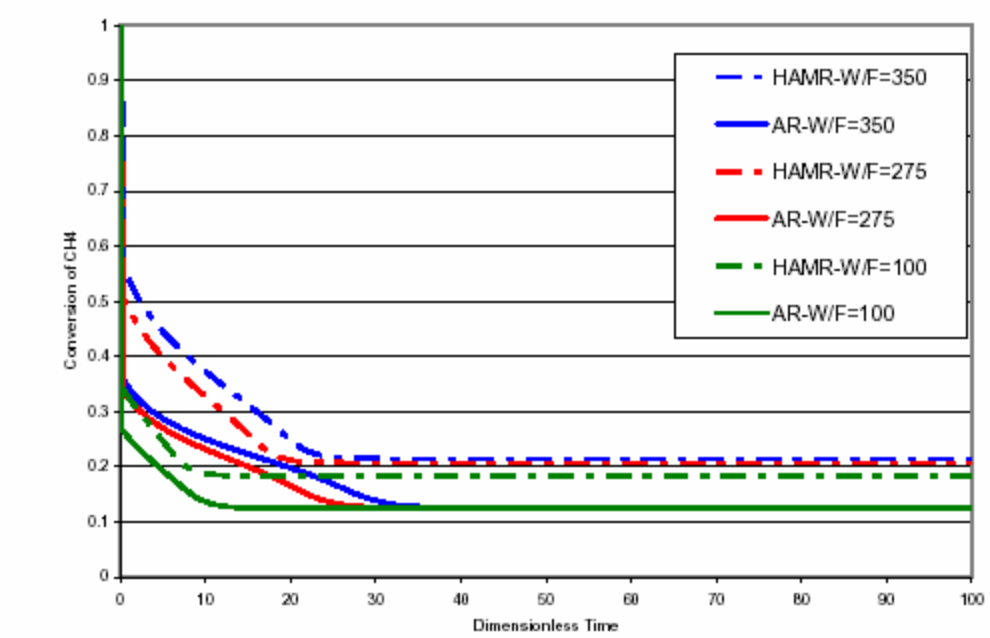

Figure 1 **Methane conversion vs dimensionless time for the invented hybrid reactor and the base case of the adsorptive reactor.**

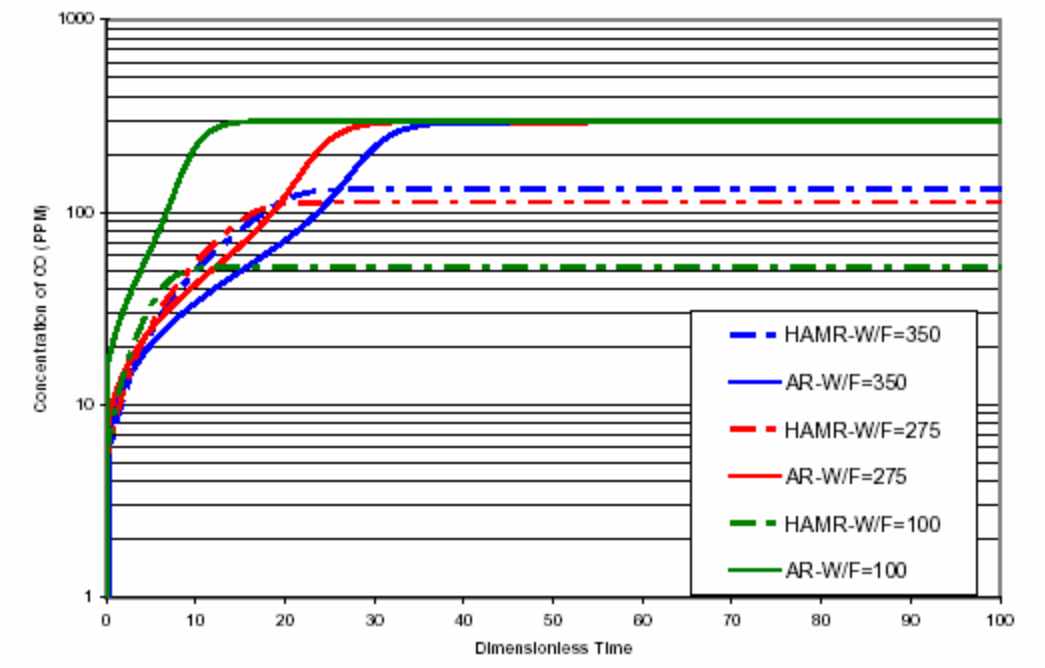

Figure 2 **Concentration of CO contaminant in the hydrogen produced from the invented hybrid reactor vs the base case of the adsorptive reactor.**

6. Experimental Verification of Invented Process

6.1. Permeance and Selectivity Measurement of Membrane under Proposed Environment

A palladium membrane supported on our ceramic substrate prepared by us was selected for this study based upon:

- Palladium membrane has been known for its extremely high permselectivity for hydrogen. For the purpose of producing a high purity for PEM type fuel cell applications, a membrane with an excellent permselectivity is a must.

- Palladium membrane shows thermal and hydrothermal stability at the proposed application temperature, i.e., 400 to 500C.

After the membrane was fabricated, single component permeation study is performed to determine its hydrogen selectivity over other gas involved in this study, including CO, CO2, water, and methane. Table 1 below presents the single component permeances and their ideal selectivity at 30 and 60 psi and 400C. Key observations include:

- The hydrogen permeance is in the range of 6 m^3/m^2/hr/bar**0.5, which is considered the high end of the range of the published hydrogen permeances by this type of membrane.
- The selectivity for hydrogen over other gas components is in the range of ~100. Although this level of selectivity is considered moderate in comparison with the published literature. However, this level of selectivity is more than adequate for the proposed application according to the mathematical simulation.
- The permeance for other gas components, including CO, CO2 and CH4 (substituted with N2), follow the trend of Knudsen diffusion. Theoretically the selectivity of hydrogen over these components by the palladium membrane is infinite. Obviously the very slight permenace measured here is most likely resulted from the defect of the membrane.
- The permeances measured from the shell vs tube sides are similar as expected. In this study we packed the catalyst on the shell side. Thus, the permeance measured from the shell side will be followed.

Table 1 Single component permeances of hydrogen, CO, CO_2, N_2 and Ar of the Palladium membrane prepared for this tudy.

Pd-01

Surface area : 0.002793(m2)

Pd-01

08-18-2005

Shell Side Feeding

Pure Gas

	400 C / 30 psig			400 C / 60 psig		
	Permeate (cc/sec)	Permeance [m3/(m2*hr*bar)]	S.F. based on H2	Permeate (cc/sec)	Permeance [m3/(m2*hr*bar)]	S.F. based on H2
H2*	5.6022	5.0884	1.0	10.5263	6.7605	1.0
CO	0.1098	0.0684	74.4	0.2358	0.0735	92.0
CO2	0.0850	0.0530	96.1	0.1878	0.0585	115.5
CH4						
H2O						
N2	0.1094	0.0682	74.6	0.2353	0.0733	92.2
Ar	0.0859	0.0536	95.0			

Pd-01

08-18-2005

Tube Side Feeding

Pure Gas

	400 C / 30 psig			400 C / 60 psig		
	Permeate (cc/sec)	Permeance [m3/(m2*hr*bar)]	S.F. based on H2	Permeate (cc/sec)	Permeance [m3/(m2*hr*bar)]	S.F. based on H2
H2*	5.0251	4.5642	1.0	9.5694	6.1459	1.0
CO	0.1071	0.0668	68.4	0.2326	0.0725	84.8
CO2	0.0746	0.0465	98.1	0.1883	0.0587	104.7
CH4						
H2O						
N2	0.1036	0.0646	70.6	0.2342	0.0730	84.2
Ar	0.0875	0.0545	83.7			

Pd-01

08-25-2005

Shell Side Feeding

Pure Gas

	400 C / 30 psig					
	Permeate (cc/sec)	Permeance [m3/(m2*hr*bar)]	S.F. based on H2	Permeate (cc/sec)	Permeance [m3/(m2*hr*bar)]	S.F. based on H2
H2*	5.4054	5.3466	1.0			
CO	0.1095	0.0683	78.3			
CO2	0.0884	0.0551	97.0			
CH4						
H2O						
N2	0.1121	0.0699	76.5			
Ar	0.0926	0.0577	92.6			

* The unit of H2 permeance is [m3/(m2*hr*bar^0.5)]

6.2. Adsorption Isotherms under Proposed Application Environment

In our invented process, adsorbent plays a role of removing CO_2, one of the two key reaction products. Thus, a reliable adsorption isothem is critical to be able to predict the reactor performance reliably. In this project, we experimentally perform the adsorption of CO_2 with hydrotalcite as the adsorbent at 400 and 450°C with the pressure ranging from 1 to 6 bar, covering the potential operating conditions. Table 2 lists the experimental results of the CO2 uptake by the hydrotalcite adsorbent. The results are also presented in Figure 3. Evidently, the CO_2 uptake at this temperature range, i.e., 400 to 450°C, is insignificant. The CO2 uptake in this study can be fited well to a Freundlic adsorption isotherm as shown in Figure 4. In addition, our invented process will operate the adsorbent under a pressure swing adsorption (PSA) mode. Thus, the adsorption capacity under a cyclic adsorption and desorption operation is evalauted. As shown in Table 3, about 5% adsorption capacity loss during the first cycle and then the capacity reaches a steady state. Thus, our experimental result on cyclic adsorption confirms that the adsorbent used in this study is qualified for the proposed operation.

Table 2 CO_2 uptake by hydrotalcite adsorbent at 400 and 450°C.

Press(atm)	Amount Adsorbed (mmol/gm), 400C	Amount Adsorbed (mmol/gm), 450C
1.0166	0.3148	0.2707
2.7429	1.4105	1.2205
4.4692	2.7515	2.5988
6.1955	4.4873	4.3650
Sample Size: 10 gm.		

Figure 3 CO_2 uptake by hydrotalcite adsorbent at 400 and 450°C

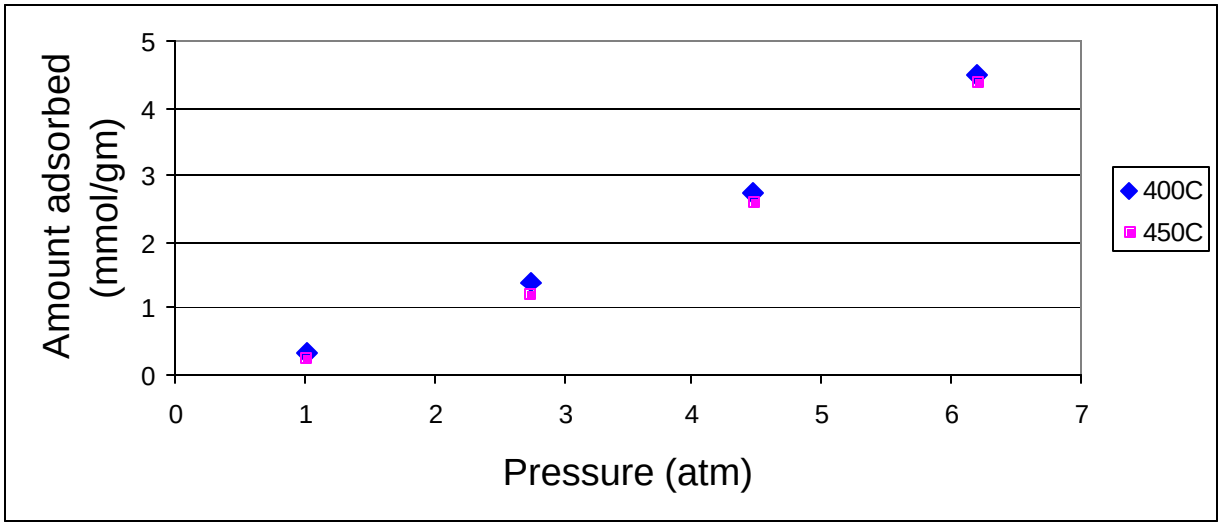

Figure 4 Adsorption isotherm of CO_2 on hydrotalcite fitted with Freundlich equation

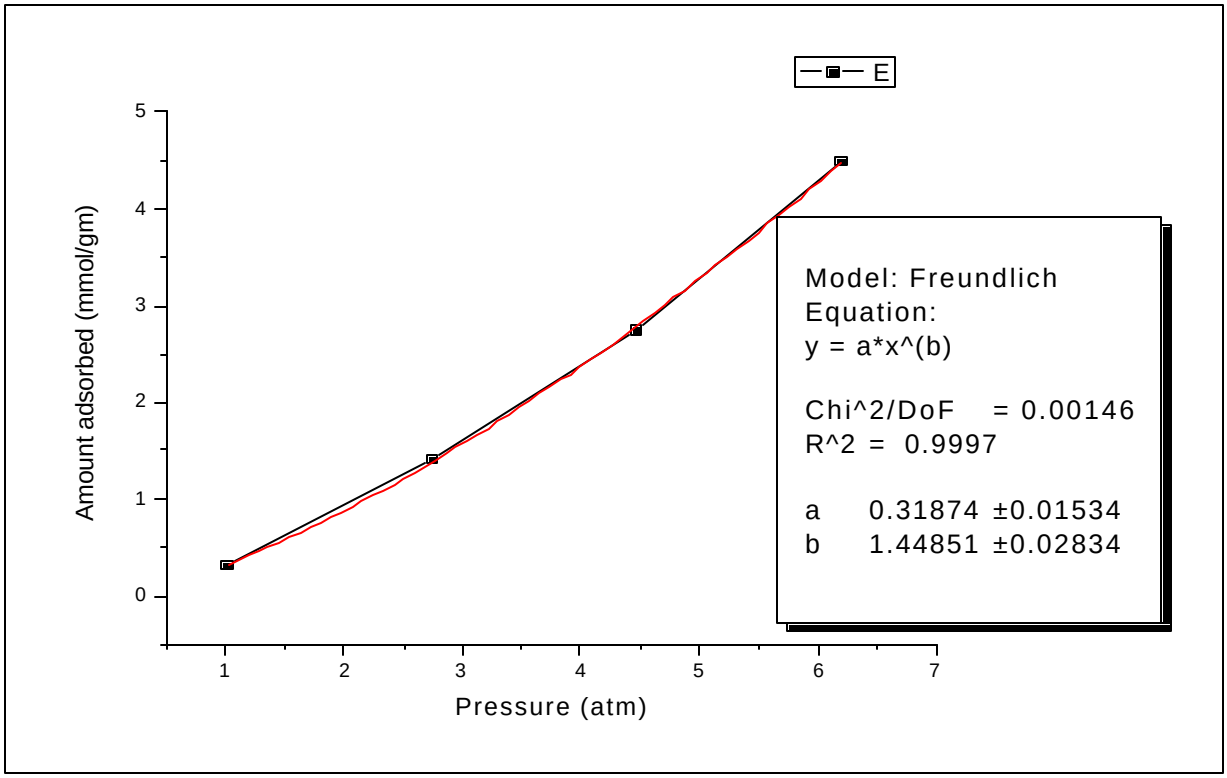

Table 3 Cyclic adsorption of CO_2 with hydrotalcite at 450°C and 1 bar.

Cycle	Press(atm)	mmol/gm
0	0	0
1	1.0166	0.323979
2	1.0166	0.309252
3	1.0166	0.307411
4	1.0166	0.309252

6.3. Reaction Kinetics under Proposed Application Environment

Steam reforming kinetic study was performed in a packed bed for the determination of the reaction kinetics, which is part of the input parameters of the mathematical model developed for the invented process. Although many steam reforming reaction rate data can be found in the literature, we have not found the data generated at the temperature range interested to us, i.e., 350 to 400°C. Table 4 summarizes the methane conversion at 350 and 400°C for the W/F ranging from100 to 500 g-mol/hr. The data were verified with the carbon balance check. All the experimental data sets except one at xxx show excellent carbon balance within 0 to 2%. Further, the methane conversion experimentally obtained was compared with the calculated conversion based upon thermodynamic calculation. Obviously the experimentally condition chosen for the study at both temperatures can deliver the conversion near thermodynamic equilibrium implies that the experimental condition chosen here is ideal to showcase the proposed process. Methane conversion beyond the thermodynamic limit can be determined reliably based upon the difference in conversion between the membrane reactor, membrane and adsorption reactor vs. the packed bed reactor.

Table 4 Methane steam reforming via a membrane reactor at 400°C.

CH4:H2O:H2 = 1.0 : 4.0 : 0.1								
Date:	7/15/2005							
Pressure(psig)	40							
T = 350 C								
W/F (g*hr/mol)		H2	CH4	CO	CO2	H2O	CH4 Conversion	% loss based on C
497.8	Feed	3.21E-03	3.21E-02	0.00E+00	0.00E+00	1.29E-01	8.76	-1.71
	Exit	1.32E-02	2.93E-02	6.72E-04	2.69E-03	0.00E+00		
248.9	Feed	6.43E-03	6.43E-02	0.00E+00	0.00E+00	2.57E-01	8.53	-1.91
	Exit	2.50E-02	5.88E-02	1.31E-03	5.40E-03	0.00E+00		
165.9	Feed	9.64E-03	9.64E-02	0.00E+00	0.00E+00	3.86E-01	7.79	1.98
	Exit	2.28E-02	8.89E-02	1.60E-03	3.99E-03	0.00E+00		
124.4	Feed	1.29E-02	1.29E-01	0.00E+00	0.00E+00	5.14E-01	7.40	0.98
	Exit	3.02E-02	1.20E-01	2.03E-03	5.76E-03	0.00E+00		
99.6	Feed	1.61E-02	1.61E-01	0.00E+00	0.00E+00	6.43E-01	5.73	-0.47
	Exit	3.62E-02	1.52E-01	3.04E-03	6.92E-03	0.00E+00		
**Equil. Conversion at 350 C for CH4 : H2O : H2 = 1.0 : 4.0 : 0.1					6.84%			
**Equil. Conversion at 350 C for CH4 : H2O : H2 = 1.0 : 4.0 : 0.0					8.67%			
T = 400 C								
W/F (g*hr/mol)		H2 (mol/hr)	CH4 (mol/hr)	CO (mol/hr)	CO2 (mol/hr)	H2O (mol/hr)	CH4 Conversion	% loss based on C
497.8	Feed	3.21E-03	3.21E-02	0.00E+00	0.00E+00	1.29E-01	14.43	-5.34
	Exit	3.24E-02	2.75E-02	1.82E-03	4.53E-03	0.00E+00		
248.9	Feed	6.43E-03	6.43E-02	0.00E+00	0.00E+00	2.57E-01	14.36	2.18
	Exit	3.68E-02	5.51E-02	1.65E-03	6.18E-03	0.00E+00		
165.9	Feed	9.64E-03	9.64E-02	0.00E+00	0.00E+00	3.86E-01	13.80	2.57
	Exit	4.17E-02	8.31E-02	2.47E-03	8.35E-03	0.00E+00		
124.4	Feed	1.29E-02	1.29E-01	0.00E+00	0.00E+00	5.14E-01	12.43	1.40
	Exit	5.81E-02	1.13E-01	1.86E-03	1.23E-02	0.00E+00		
99.6	Feed	1.61E-02	1.61E-01	0.00E+00	0.00E+00	6.43E-01	11.43	0.11
	Exit	6.29E-02	1.42E-01	3.86E-03	1.43E-02	0.00E+00		
**Equil. Conversion at 400 C for CH4 : H2O : H2 = 1.0 : 4.0 : 0.1					12.80%			
**Equil. Conversion at 400 C for CH4 : H2O : H2 = 1.0 : 4.0 : 0.0					14.60%			

The above conversion results obtained for a packed bed reactor were used to derive the reaction rate kinetic data based upon the equations detailed in Appendix.

6.4. Experimental Verification of the Invented Process

Table 5 Methane steam reforming via a membrane reactor at 400°C.

Feed side :: CH4 : H2O : H2 = 1.0 : 4.0 : 0.1								
Permeate side :: 0.5*(total feed) H2O								
Date:	8/31/2005							
Pressure(psig)	40							
Temp.(C)	400							
Membrane	Pd-01							
W/F (g*hr/mol)		**H2 (mol/hr)**	**CH4 (mol/hr)**	**CO (mol/hr)**	**CO2 (mol/hr)**	**H2O (mol/hr)**	**CH4 Conversion**	**% loss based on C**
124.4	**Feed**	**1.61E-02**	**1.61E-01**	**0.00E+00**	**0.00E+00**	**6.43E-01**	**16.53**	**-1.43**
	Reject	9.69E-02	1.01E-01	6.90E-03	1.27E-02	0.00E+00		
	Permeate	2.74E-02	3.35E-02	2.12E-03	7.12E-03	0.00E+00		
103.7	**Feed**	**1.93E-02**	**1.93E-01**	**0.00E+00**	**0.00E+00**	**7.71E-01**	**16.69**	**-4.54**
	Reject	8.68E-02	8.53E-02	5.20E-03	1.35E-02	0.00E+00		
	Permeate	6.32E-02	7.53E-02	4.73E-03	1.75E-02	0.00E+00		
88.9	**Feed**	**2.25E-02**	**2.25E-01**	**0.00E+00**	**0.00E+00**	**9.00E-01**	**16.19**	**-3.21**
	Reject	7.96E-02	8.48E-02	4.66E-03	9.53E-03	0.00E+00		
	Permeate	8.69E-02	1.04E-01	6.61E-03	2.29E-02	0.00E+00		
62.2	**Feed**	**3.21E-02**	**3.21E-01**	**0.00E+00**	**0.00E+00**	**1.29E+00**	**11.67**	**-2.62**
	Reject	6.78E-02	8.94E-02	4.58E-03	9.11E-03	0.00E+00		
	Permeate	1.01E-01	1.94E-01	9.44E-03	2.28E-02	0.00E+00		
Equil. Conversion for CH4 : H2O : H2 = 1.0 : 4.0 : 0.1					12.80%			

7. Economic Analysis of Invented Process

7.1. Product Costs based upon Our Invented vs Competitive Process

Our comparison here is limited to the capital cost for hydrogen production for distributed/stationary applications. Thus far, no technology development for vehicle applications has been advanced enough for reliable product cost analysis. Discussion on energy savings is made in Criterion #3 next. Although the processes for conventional vs our invented reforming is very similar, there are two fundamental differences. First, the conventional SMR and WGS reactors and CO post-treatment are replaced by our invented process with a single stage reformer/separator. Second, heat for the endothermic reaction is supplied to the reactor in the form of a steam sweep of the permeate side of the membrane. By comparison, in the conventional SMR reactor, flue gas from the burner is used directly to provide this reaction heat [11].

The table below presents the estimated capital cost of the conventional process for small scale distributed production of 2,000 scfh of H_2[11] and compares this with our invented alternative.

The total capital cost for our invented process is about 50% of that required for the conventional reactor. The primary reason for this is the lower reactor cost and the elimination of the downstream unit operations, particularly H_2 purification via PSA. It should be noted that the H_2 yield in the conventional SMR with PSA capital system is about 75% vs. >95% with our proposed process. Hence, the proposed process would produce 2500 SCFH H_2 vs. 2000 SCFH for the conventional system.

Unit Operation	Conventional SMR/WGS [$]	M&P Process [$]
Gas Compressor	2,300	2,300
HDS including preheater	4,400	4,400
Water Boiler w/superheater	13,600	9,600
SMR including burner (800ºC)	29,300	0
Reactor Catalyst	2,000	2,000
HTS Reactor (400ºC)	15,400	0
M&P Reactor	0	19,000
M&P Burner	0	2000
Air Cooler 1	4,300	0
Air Cooler 2	3,000	0
Permeate Condenser	0	7,000
Water Preheater	0	3,000
H_2 Separator (PSA: <10 ppm CO)	18,800	0
Total Cost [$]	**93,100**	**49,300**
H_2 Produced [SCFH]	2000	2500

7.2. Energy Savings

\

Please refer to Appendx E for Energy Savings Metrics

7.3. Economical and Environmental Benefits

The use of automobiles and light trucks in US accounts for 40% of the total petroleum consumption. The transportation sector relies on petroleum for 97% of its energy and over half of this comes from foreign sources[3], which has energy security implications. According to the DOE estimate, the future high efficiency vehicles with fuel cells and other improvements will achieve 3 time reduction in fuel consumption[2]. About 25% of the total petroleum consumption can be saved with the implementation of this proposed technology. This is equivalent to ~5 million barrels/day petroleum usage reduction, or 50% reduction in US petroleum import. In addition, the transportation sector contributes air pollution substantially[3]. Highway road vehicle emissions account for about 27% of man-made volatile organic compound emissions, 32% of

[3] US DOE Solicitation No. DE-PS36-03GO93007, July 24, 2003

nitrogen oxide emissions, and 62% of CO emissions on an annual basis in the USA. The proposed technology offers hydrogen supply via on-board reforming or via refueling stations. This would eliminate one of the key challenges facing the implementation of the fuel cell technology in the transportation sector, resulting in reducing or eliminating these pollutants. Organic compound emissions from these vehicles would be reduced dramatically, about 80%, since no more than 25% hydrocarbon fuels are unconverted, which are combusted for heat recovery applications. 3 time reduction in CO_2 is expected due to its reduced fuel usage, which can be concentrated in a reject stream ready for sequestration. Finally the quality of life would be improved as a result of several intangible benefits, such as noise reduction through the use of fuel cells in vehicles, back-up power by fuel cell to dampen the peak electricity load, and others.

7.4. Conclusions

Our project involves the bench-scale demonstration of a high-efficiency low-temperature steam reforming process. Hydrogen production can be operated at 350 to 400ºC with our invention, as opposed to >800ºC of existing reforming. Several conclusions can be drawn based upon the experimental study performed under this project:

- *Ceramic Membrane deposited with Pd thin prepared by us was found suitable for proposed application environment. In addition, its permeance and selectivity were found adequate for the invented process.* Its permeance for hydrogen at 450C is about 10 $m^3/m^2/hr/bar^{0.5}$. The selectivity is about 100 for hydrogen over CO, CO_2, and N_2 (a substitute for methane) based upon the single component permeance measurement. The permeances for CO, CO_2 and N_2 are believed to be resulted from defects of the membrane/leaks of the module because Knudsen diffusion trends were followed for these components.

- *Hydrotalcite prepared by us was found adequate for the adsorption of CO_2 for the invented process.* The adsorption isotherm for the selected hydrotalcite adsorbent was determined experimentally at 400 and 450°C and up to 6 bar. The capacity in the neighborhood of 0.3 mmol/g at 1 bar and >4 mmol/g at 6 bar. A Freundlich adsorption isotherm was applied to describe well the CO_2 uptake vs pressure. Further, the capacity loss under cyclic adsorption/desorption was confirmed very insignificant, i.e., <5% loss after the 1^{st} cycle and negligible for $>1^{st}$ cycle.

- *A commercial steam reforming catalyst was used to generate the reaction kinetic parameters required for the proposed operating condition at 350 and 400°C.* Although the reaction temperature is low and no literature data is available, we were able to reach the thermodynamic conversion in a packed bed under the proposed operating condition. This implies that the reaction kinetics with the commercial catalyst at this extremely low temperature is adequate for the invented process.

- *According to our simulation with the input parameters obtained experimentally above, our invented hybrid process can deliver 35 to 55% methane conversion, in comparison with the 12 and 18-21% conversion of the packed bed and an adsorptive reactor respectively.* In addition CO contamination with <10 to 120 ppm is predicted for the

invented process depending upon the cycle time for the PSA type operation. In comparison, the adsorption reactor can also deliver a similar CO contaminant at the low end; however, its CO contamination at the high end reaches as high as 300 ppm based upon the simulation of our proposed operating condition.

- Our experimental results for the packed bed and the membrane reactor deliver 12 and 18% conversion respectively at 400°C, approaching the conversion by the mathematical simulation. Due to the time constraint, the experimental study on the conversion of the invented process has not been complete. However, our in-house study using a similar process concept for the water gas shift reaction has demonstrated the reliability of our mathematical simulation for the invented process. In summary, we are confident that the invented process can deliver efficiently high purity hydrogen at a low temperature (~400°C).

- According to our projection, the invented process can further achieve 5% energy savings and ~50% capital savings over conventional reforming for fuel cell applications. The pollution abatement potential associated with the implementation of fuel cells, including the elimination of nitrogen oxides and CO, and the reduction in volatile organics and CO_2, can thus be realized with the implementation of this invented process. The projected total market size for equipment sale for the proposed process in US is $1.5 billion annually.

Due to the positive results obtained thus far, it is recommended to complete the experimental study to verify the simulation results. Further, a process optimization task can be pursued to determine the maximum energy and capital cost savings possibly achieved by the invented process.

Appendix A

Final Task Schedule

Task Schedule

Task Number	Task Description	Task Completion Date				Progress Notes
		Original Planned	Revised Planned	Actual	Percent Complete	
1	Construction of Bench-Scale Testing Unit	10/31/04	12/31/04	12/31/04	100%	Completed.
2	Refining Mathematical Model	12/31/04	2/28/05	2/28/05	100%	Completed
3	Experimental Verification of Invented Process	5/31/05	8/31/05	9/30/05	95%	In progress
4	Process Simulation, Optimization and Economic Analysis	6/31/05	8/30/05	9/30/05	100%	Completed

Appendix B

Final Spending Schedule

Appendix C

Final Cost Share Contributions

Cost Share Contributions

Funding Source	Approved Cost Share		This Quarter		Cumulative to Date	
	Cash	In-Kind	Cash	In-Kind	Cash	In-Kind
Cumulative Cost Share Contributions					0.00	

Appendix D

Energy Sagings Metrics

One Unit of Propsoed Technology:

2,000 scfh of H_2 production for the proposed technology for small scale distributed hydrogen production applications.

One Unit of Current Technology:

2,000 scfh of H_2 for convetional process for small sclae distributed hydrogen production

Energy Savings Metrics

The total hydrogen required for transportation is based upon hydrogen consumption to power the future high efficiency vehicles in US. Total energy savings by the invented process are summarized below:

Category / Region	Hydrogen Required for Transportation [mol H_2/yr]	Energy Savings by Proposed Invention [Btu/mol H_2]		Total Energy Savings [Btu/yr]
		Sensible Heat Savings	Heat Recovery Savings	
US	21×10^{12}	6.3	2.5	185×10^{12}
Worldwide	42×10^{12}	6.3	2.5	370×10^{12}

Based upon the process scheme and the simulation result (see Sec. 6), potential energy savings resulting from replacing existing steam reforming with our invented process for distributed/stationary/on-board hydrogen production are derived from three areas below:

- our proposed reformer operated at 350 to 400°C vs >800°C of existing commerical SMR,
- more cost-effective heat recovery and utilization of steam requirement for reaction, and
- elimination of several major unit operations for post treatment.

The energy saving calculation here is limited to the first two factors resulting from the reactor operating temperature difference. Energy savings due to the elimination of some unit operations required for post treament (the 3rd factor) is not as significant as the refomer, and is not taken into consideration here. Thus, the energy saving estimate presented below should be considered as a minimum saving case.

Calculation for Hydrogen Required for Transportation

- The total hydrogen requirement is calculated based upon reforming the moles of methane-equivalent requried to power high effiency vehicles (see definition below). Thus, savings are made based upon the comparison of existing vs proposing steam reforming process to supply

hydrogen required for the transportation sector using gasoline. Diesel powered vehicles are not accounted for in this calculation.

- Total US gasoline consumption is ~9 million barrel per day currently[1]. About 95% is used by transporation[2]. This amounts to $43x10^{12}$ Btu per day.
- The future high-effiency vehicle with fuel cells and other improvements will result in 3 time reduction in energy consumption[2]. Thus, the methane-equivalent consumption for the future vehicle in US is 57×10^9 mole /day on equal Btu basis.
- The global energy consumption is assumed to be double of the comsumption in US.

Calculation for Energy Savings resulting from Sensible Heat Difference

- 75% conversion of hydrocarbon feed to hydrogen by steam reforming is assumed for both existing and proposed reforming technologies. Also 4 moles steam is requried for each mole of methane.
- The energy savings from the sensible heat difference (400 vs 800ºC) is straightforward to calculate and is approximately 6.3 Btu/mol H_2 produced.

Calulation for Energy Savings resulting from Heat Recovery

- Starting with the conventional reactor, approximately 13 Btu per mol of produced H_2 is recovered from the reactor effluent via steam generation. Of this, 5.3 Btu/mol H_2 is injected into the natural gas feed. In a refinery, the remaining 7.7 Btu/mol is "exported" [11]. However, to provide water to the reaction, it is not likely that this "export" steam could be used for small reformers for on-board or distributed H_2 generation. Hence, this would simply be an energy loss.
- The total quantity of steam generated is expected to be less for our invented process due to the lower reaction temperature. However, more aggressive heat recovery can be practiced in our proposed process. The heat exchanger materials of construction are less exotic at =400°C (vs 800°C). Further, no high and low temperature water gas shift reactions are required in the invented process. Hence it is reasonable to estimate that up to an additonal 20% of the heat lost (i.e., not recovered) in the conventional reactor can be recovered in the proposed process. Given these adjustments, it is estimated that the invented process would save an additional 2.5 Btu/mol H_2 in comparison to the conventional SMR.

In summary, the implementation of the fuel cell technology in transportation will achieve three time reduction of current transportation energy usage according to DOE objective. This amounts to 11×10^{15} Btu/yr savings in US. Our proposed process offers a technical feasible solution for this application. On top of that, our invented process will achieve 185×10^{12} Btu/yr savings over conventional reforming. This amounts to ~5% savings of the reduced energy consumption (i.e., after 3 time reduction by the implementation of the fuel cell in vehicles). In addition, about 50% capital cost reduction can be achieved with our proposed process as discussed above.

[1] Personal communication with D. Kosowski, Refining Process Service, Pittsburgh, PA
[2] US DOE Solicitation No. DE-RP04-01AL67057, November 21, 2000

Supplemental Information attached below:

Design Aspects of Hybrid Adsorbent−Membrane Reactors for Hydrogen Production

Babak Fayyaz,[†] Aadesh Harale,[†] Byoung-Gi Park,[‡] Paul K. T. Liu,[§] Muhammad Sahimi,[†] and Theodore T. Tsotsis*[,†]

Department of Chemical Engineering, University of Southern California, Los Angeles, California 90089-1211, LG Petrochemical Company, Ltd., LG Twin Towers, Youido, P.O. Box 672, Seoul, Republic of Korea, and Media and Process Technology, Inc., Pittsburgh, Pennsylvania 15236

We present a detailed investigation of the design characteristics and performance of a novel reactor system, termed the hybrid adsorbent−membrane reactor (HAMR), for hydrogen production. The HAMR concept, originally proposed by our group[1,2] for esterification reactions, couples the reaction and membrane separation steps with adsorption on the membrane feed or permeate side. The HAMR system investigated previously involved a hybrid pervaporation membrane reactor and integrated the reaction and pervaporation steps through a membrane with water adsorption. Coupling reaction, pervaporation, and adsorption significantly improved the performance. In this paper, we investigate a new HAMR system involving a hybrid packed-bed catalytic membrane reactor coupling the methane-steam-reforming reaction through a porous ceramic membrane with a CO_2 adsorption system. The present HAMR system is of potential interest to pure hydrogen production for proton exchange membrane (PEM) fuel cells for various mobile and stationary applications. The reactor characteristics have been investigated for a range of temperature and pressure conditions relevant to the aforementioned applications. The HAMR system exhibits enhanced methane conversion, hydrogen yield, and product purity and shows good promise for reducing the hostile operating conditions of conventional methane−steam reformers and for meeting the product purity requirements for PEM operation.

1. Introduction

As a result of stricter environmental regulations worldwide, hydrogen is progressively becoming a very important clean energy source for both mobile and stationary applications. For hydrogen to replace fossil fuels as the fuel of choice for mobile applications, it will require the creation of a production and delivery infrastructure equivalent to those that currently exist for fossil fuels. As an alternative and an interim step toward the new hydrogen economy, various groups are currently investigating hydrocarbon steam reforming for onboard generation of hydrogen for use in fuel-cell-powered vehicles, or for on-site production, in place of compressed or liquid hydrogen gas storage for stationary power generation applications.[3−6] Methane−steam reforming is currently attracting renewed interest in this regard, particularly for distributed power generation through the use of fuel cells. The process is widely practiced for large-scale hydrogen production and involves reacting steam with methane, through the endothermic and reversible methane−steam-reforming reaction, over supported nickel catalysts in packed-bed reactors (reformers). Traditionally, these reformers have generally operated at temperatures often in excess of 1000 K and pressures as high as 30 bar and reach relatively low equilibrium conversions.[7−9] Such conditions are often neither convenient nor economical to attain for small-scale, on-site (or onboard) hydrogen generation. As a result, there is much current interest in the development of more effective reforming technologies.

Reactive separation processes have been attracting renewed interest for application in catalytic steam reforming. They include packed-bed catalytic membrane reactors (MRs)[10−15] and, more recently, absorptive reactor (AR) processes.[16−26] Their potential advantages over the more conventional reformers have been widely discussed. They include (i) increasing the reactant conversion and product yield, through shifting of the equilibrium toward the products, potentially allowing one to operate under milder operating conditions (e.g., lower temperatures and pressures and reduced steam consumption), and (ii) reducing the downstream purification requirements by in situ separating from the reaction mixture the desired product hydrogen (in the case of MRs) or the undesired product CO_2 (in the case of ARs).

MRs show substantial promise in this area and, typically, utilize nanoporous inorganic or metallic Pd or Pd−alloy membranes.[15] The latter are better suited for pure hydrogen production. However, metallic membranes are very expensive and become brittle during reactor operation[13] or deactivate in the presence of sulfur or coke. Nanoporous membranes are better suited for the steam-reforming environment. They are difficult to manufacture, however, without cracks and pinholes and, as a result, often have inferior product yield. In addition, the hydrogen product in the permeate side contains substantial amounts of other byproducts, particularly CO_2, and may require further treatment for use in fuel-cell-powered vehicles.

Adsorptive methane−steam-reforming reactors also show good potential.[16−20] The challenge here, however, is in matching the adsorbent properties with those of the catalytic system. Two types of adsorbents have been suggested: potassium-promoted layered-double hydroxides (LDHs), which operate stably only at lower tem-

* To whom correspondence should be addressed. Tel.: (213) 740-2069. Fax: (213) 740-8053. E-mail: tsotsis@usc.edu.
[†] University of Southern California.
[‡] LG Petrochemical Co., Ltd.
[§] Media and Process Technology, Inc.

10.1021/ie050199u CCC: $30.25
Published on Web 00/00/0000 **PAGE EST: 10.5**

Table 1. Rate Expressions and Thermodynamic Properties for the Methane−Steam-Reforming Reaction[a,8]

i	reaction	rate expression	heat of reaction at 298 K, ΔH_R^0 (kJ/mol)	equilibrium constant, K_{eqi}
1	$CH_4 + H_2O \leftrightarrow CO + 3H_2$	$r_1 = (k_1/P_{H_2}^{2.5})(P_{CH_4}P_{H_2O} - P_{H_2}^3P_{CO}/K_{eq1})/DEN^2$	206.1	$K_{eq1} = \exp[30.114 - 26830/T]$
2	$CO + H_2O \leftrightarrow CO_2 + H_2$	$r_2 = (k_2/P_{H_2})(P_{CO}P_{H_2O} - P_{H_2}P_{CO_2}/K_{eq2})/DEN^2$	−41.15	$K_{eq2} = \exp[-4.036 + 4400/T]$
3	$CH_4 + 2H_2O \leftrightarrow CO_2 + 4H_2$	$r_3 = (k_3/P_{H_2}^{3.5})(P_{CH_4}P_{H_2O}^2 - P_{H_2}^4P_{CO_2}/K_{eq3})/DEN^2$	164.9	$K_{eq3} = K_{eq1}K_{eq2}$

[a] $DEN = 1 + K_{CO}P_{CO} + K_{H_2}P_{H_2} + K_{CH_4}P_{CH_4} + K_{H_2O}P_{H_2O}/P_{H_2}$.

Table 2. Kinetic Parameters for the Methane−Steam-Reforming Reaction[8]

kinetic parameter	preexponential terms, k_{i0}, K_{i0}	activation energies or heats of chemisorption, E_a, ΔH (kJ/mol)	units
k_1	4.225×10^{15}	240.1	kmol·bar$^{0.5}$/kg of catalyst/h
k_2	1.955×10^{6}	67.13	kmol/kg of catalyst/h/bar
k_3	1.020×10^{15}	243.9	kmol·bar $^{0.5}$/kg of catalyst/h
K_{CO}	8.23×10^{-5}	−70.65	bar^{-1}
K_{H_2}	6.12×10^{-9}	−82.90	bar^{-1}
K_{CH_4}	6.65×10^{-4}	−38.28	bar^{-1}
K_{H_2O}	1.77×10^{5}	88.68	

peratures (less than 500 °C[25−27]), and CaO or commercial dolomite, which can be utilized at the typical steam-reforming temperatures of 650−700 °C[21] but requires temperatures higher than 850 °C for regeneration.[23,24] These are very harsh conditions that result in gradual deterioration of the adsorbent properties and potentially sintering of the reforming catalyst.[23,24] The mismatch between the reaction and regeneration conditions is likely to result in significant process complications.

Here, what we propose for use is a novel reactor system, termed the hybrid adsorbent−membrane reactor (HAMR). The HAMR concept, originally proposed by our group,[1,2,28] couples the reaction and membrane separation steps with adsorption on the reactor and/or membrane permeate side. The HAMR system investigated previously involved a hybrid pervaporation MR system and integrated the reaction and pervaporation steps through a membrane with water adsorption. Coupling reaction, pervaporation, and adsorption significantly improved the performance. Most recently, Elnashaie and co-workers[29−32] mathematically analyzed the behavior of a circulating fluidized-bed HAMR system utilizing Pd membranes. This reactor is assumed to operate at steady state by recirculating the catalyst and adsorbent through a second reactor for regeneration. The ability of Pd membranes to withstand the rigors of the fluidized-bed steam-reforming environment and of the adsorbents to undergo continuous recirculation and regeneration still remains the key challenge. In addition, this system is not well-suited for onboard or small-scale applications.

The HAMR configuration can be potentially used with equilibrium- or selectivity-limited reactions in which one of the products can be adsorbed while another (or the same) product can be simultaneously removed via a membrane. What limits the application of the concept is the availability of efficient adsorbents that are also stable at reaction conditions. Esterification reactions (like the ethanol reaction with acetic acid to produce ethyl acetate previously studied by our group[1,2]), through the use of water adsorbents, and the production of hydrogen (through steam reforming or the water gas shift reactions) are two key potential applications. In this paper, we investigate a HAMR system involving a hybrid packed-bed catalytic MR, coupling the methane−steam-reforming reaction through a porous ceramic membrane with a CO_2 adsorption system. This HAMR system exhibits behavior that is more advantageous than either the MRs or ARs, in terms of the attained yields and selectivities. In addition, the HAMR system potentially allows for significantly greater process flexibility than either the MR or AR system. The membrane, for example, can potentially be used to separate the catalyst from the adsorbent phase, thus allowing for in situ continuous regeneration of the adsorbent. This offers a significant advantage over the ARs, which are, by definition, discontinuous systems and require the presence of multiple beds (one being in operation while the other is being regenerated) to simulate continuous operation. The HAMR system shows, furthermore, significant potential advantages with respect to the conventional MR system. Beyond the improved yields and selectivities, the HAMR system has the potential for producing a CO-free fuel-cell-grade hydrogen product, which is of significance for the proposed fuel-cell-based mobile applications of such systems.

In this preliminary paper, a mathematical model for the HAMR system is presented and analyzed for a range of temperature and pressure conditions. The behavior of the HAMR system is compared with the conventional packed-bed reactor, as well as a MR and an AR system.

2. Theory

2.1. Kinetics for Methane−Steam Reforming. For the methane−steam reaction, we utilize a catalytic reaction scheme, first proposed by Xu and Froment,[8] that has since found widespread application. According to Xu and Froment[8] (see also Elnashaie et al.[7] and Nam et al.[13]), the methane−steam-reforming reaction consists of two major endothermic reforming reaction steps, together with the exothermic water gas shift reaction (see Table 1), with the overall reaction being highly endothermic. The rate expressions, heats of reaction, and thermodynamic constants for the three reaction steps are shown in Table 1. The kinetic parameters, as reported by Xu and Froment,[8] are shown in Table 2. Formation rates for the H_2, CO, and CO_2 products and the disappearance rates for CH_4 and H_2O are given by the following equations:

$$R_{H_2} = +3r_1 + r_2 + 4r_3 \quad (1)$$

$$R_{CO} = +r_1 - r_2 \quad (2)$$

$$R_{CO_2} = +r_2 + r_3 \quad (3)$$

$$R_{CH_4} = -r_1 - r_3 \quad (4)$$

$$R_{H_2O} = -r_1 - r_2 - 2r_3 \quad (5)$$

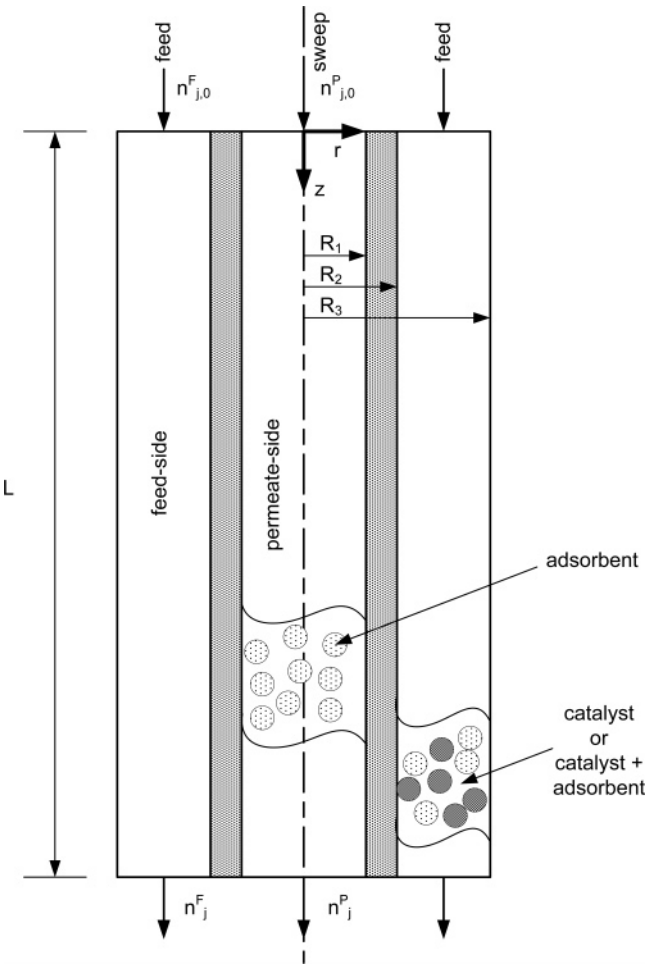

Figure 1. Schematic diagram of a HAMR system.

2.2. Mathematical Model of the HAMR System. A schematic of the HAMR system is shown in Figure 1. In this figure, the catalyst and adsorbent are packed in the exterior of the membrane (signified by the superscript F, or the feed side), with additional adsorbent also packed in the interior of the membrane volume (signified by the superscript P, or the permeate side). There are, of course, a number of other potential reactor configurations, as previously noted. For example, the catalyst may be loaded in the feed side, while the adsorbent may also be loaded in the permeate side, or the catalyst and adsorbent may only be loaded in the feed side, with no adsorbent or catalyst being present in the permeate side, which is the configuration that is analyzed here. To simplify matters, in the development of the model, we assume that the reactor operates isothermally, that external mass-transfer resistances are negligible for the transport through the membrane as well as for the catalysts, and that internal diffusion limitations for the catalyst, and internal or external transport limitations for the adsorbent, are accounted for by the overall rate coefficients. Moreover, plug-flow conditions are assumed to prevail for both the interior and exterior membrane volumes, as well as ideal gas law conditions.

In the simulations reported here, we utilize the experimentally measured transport characteristics of a microporous SiC membrane prepared by our group.[33] These membranes have been shown previously to be thermally and hydrothermally stable under conditions akin to the steam-reforming reaction conditions[33] (further details about their preparation and characterization can be found in the original publication). The SiC membranes are highly permselective toward hydrogen, with gases with larger kinetic diameters permeating only by Knudsen diffusion through membrane pinholes and cracks.[33] Mass transfer through the porous membrane is described by the following empirical equation:

$$F_j = U_j(P_j^F - P_j^P) \tag{6}$$

where F_j is the molar flux (mol/m^2·s), P_j^F the partial pressure of component j on the membrane feed side (bar), P_j^P the partial pressure of component j on the membrane permeate side (bar), and U_j the membrane permeance for component j (mol/m^2·bar·s). Equation 6 is, of course, a simplified empirical expression for describing flux through a nanoporous membrane for which the size of the pores approaches that of the diffusing molecules. Substantial efforts are currently ongoing by our group and others for a better understanding of the phenomena that occur during molecular transport through such nanoporous systems. Simple analytical expressions for describing transport through such membranes are currently lacking, however, thus the choice of the commonly utilized empirical equation 6 in this preliminary reactor modeling investigation.

The mass balance on the feed side of the reactor packed with methane−steam-reforming catalyst and, potentially, an adsorbent is described by the following equations for CO_2, CO, H_2, H_2O, CH_4, and an inert species (potentially used as a sweep gas or a blanketing agent; for catalytic steam reforming, a practical sweep gas would be either steam or hydrogen, however):

$$\epsilon^F \frac{\partial C_j^F}{\partial t} + \frac{\partial n_j^F}{\partial V} = -\alpha_m U_j(P_j^F - P_j^P) + (1 - \epsilon_b^F)\beta_c \rho_c R_j^F - (1 - \epsilon_b^F)(1 - \beta_c)\rho_a G_j^F + \epsilon_b^F (A^F)^2 \frac{\partial}{\partial V}\left(D_L^F \frac{\partial C_j^F}{\partial V}\right); \quad j = 1, 2, ..., n \tag{7}$$

In eq 7, n_j^F is the molar flow rate (mol/s) for species j and C_j^F is the gas-phase concentration (kmol/m^3) equal to n_j^F/Q^F, where Q^F is the volumetric flow rate (m^3/s). V is the feed-side reactor volume variable (m^3), A^F the cross-sectional area for the reactor feed side (m^2), α_m the membrane area per feed-side reactor volume (m^2/m^3), ϵ_b^F the bed porosity on the feed side, ϵ^F the total feed-side bed porosity (it includes the bed porosity and catalyst porosity), β_c the fraction of the solid volume occupied by catalysts ($\beta_c = 1$ when no adsorbent is present), ρ_c the catalyst density (kg/m^3), ρ_a the adsorbent density (kg/m^3), and R_j^F the reaction rate expression, which either is described by eqs 1−5 (mol/kg·s) or is equal to zero if j is an inert species. Assuming that the adsorbent only adsorbs CO_2, G_j^F is zero for all other components except CO_2. D_L^F (m^2/s) is the axial dispersion coefficient given by the following equation[34] generally applicable for describing dispersion phenomena through packed beds:

$$D_L^F = 0.73 D_m^F + \frac{0.5 u^F d_P^F}{1 + 9.49(D_m^F/u^F d_P^F)} \tag{8}$$

where D_m^F is molecular diffusivity (m^2/s), u^F is the

velocity at the feed side (m/s), and d_P^F is the particle diameter in the feed side (m).

One finds a number of approaches in the literature for describing $G_{CO_2}^F$. Ideally, one would like to account explicitly for both external and internal mass transport and finite rates of adsorption. Such an approach goes beyond the scope of this preliminary investigation, however, in addition to the fact that there are currently no experimental high-temperature transport/adsorption CO_2 data to justify this level of mathematical detail. Traditionally, in the modeling of ARs, simpler models have been utilized instead.[22,27] Two such models have received the most attention. They are (i) the model based on the assumption of an instantaneous local adsorption equilibrium between the gas and adsorbent phases[2,22,27,28] and (ii) the linear driving force (LDF) models, according to which[35] $G_{CO_2}^F$ is described by the following expression:

$$\frac{dC_s}{dt} = G_{CO_2}^F = k_a(C_{seq} - C_s) \tag{9}$$

where C_{seq} is the adsorption equilibrium CO_2 concentration on the adsorbent (mol/kg) corresponding to the prevailing gas-phase concentration, C_s is the existing adsorbed CO_2 concentration (mol/kg), and k_a (s^{-1}) is a parameter that "lumps" together the effects of external and intraparticle mass transport and the sorption processes and that, as a result, is often a strong function of temperature and pressure,[27] although, typically, in modeling it is taken as temperature/pressure-independent. To calculate C_{seq}, we utilize the data reported by Ding and Alpay[22,27] for CO_2 adsorption on potassium-promoted LDH. They showed that the CO_2 adsorption on this adsorbent follows a Langmuir adsorption isotherm under both dry and wet conditions, described by the following equation:

$$C_{seq} = \frac{m_{CO_2} b_{CO_2} P_{CO_2}}{1 + b_{CO_2} P_{CO_2}} \tag{10}$$

where m_{CO_2} (mol/kg) is the total adsorbent capacity and b_{CO_2} (bar^{-1}) the adsorption equilibrium constant, which is described by the van't Hoff equation:

$$b_{CO_2} = b_{CO_2}(T_0)\exp[-\Delta H_a/R(1/T - 1/T_0)] \tag{11}$$

The heat of adsorption, ΔH_a (kJ/mol), under wet conditions for a region of temperatures from 481 to 753 K was calculated to be −17 kJ/mol, while b_{CO_2} at 673 K is equal to 23.6 bar.[27] Equations 7 and 9 must be complemented by initial and boundary conditions. For simplicity, we assume here that the reactor, prior to the initiation of the reaction/adsorption step, has undergone a start-up procedure as described by Ding and Alpay[22] that involves (i) heating the reactor to the desired temperature under atmospheric pressures by feeding H_2 on the reactor feed side and the chosen sweep gas on the permeate side, (ii) supplying water to the system so that the feed H_2O/H_2 ratio is the same as the H_2O/CH_4 ratio to be used during the reaction step, (iii) pressurizing the feed and permeate sides to the desired pressure conditions, and (iv) switching from H_2 to CH_4 to initiate the reaction/adsorption step. In the simulations, the conditions prevailing at the start of step iv are those prevailing at steady state during step iii. In addition, during step iv the following conventional boundary conditions prevail:[16–20]

$$\text{at } V = 0; \qquad \frac{\partial x_j^F}{\partial V} = -\frac{u_0^F(x_{j0}^F - x_j^F)}{A^F \epsilon_b^F D_L^F} \tag{12a}$$

$$\text{at } V = V_R; \qquad \partial x_j^F/\partial V = 0 \tag{12b}$$

where u_0^F is the inlet superficial velocity (m/s), V_R the total reactor volume (m^3), x_j^F the mole fraction, and x_{j0}^F the inlet mole fraction for species j.

Assuming that the catalyst and adsorbent particles have the same size, the pressure drop in a packed bed can be calculated using the Ergun equation:

$$-\frac{dP^F}{dV} = 10^{-6}\frac{f^F(G_m^F)^2}{A^F g_c d_P^F \rho_F^F} \tag{13}$$

$$\text{at } V = 0, \quad P^F = P_0^F \tag{13a}$$

$$f^F = \left(\frac{1 - \epsilon_b^F}{(\epsilon_b^F)^3}\right)\left(1.75 + \frac{150(1 - \epsilon_b^F)}{N_{Re}^F}\right) \tag{13b}$$

$$N_{Re}^F < 500(1 - \epsilon_b^F) \tag{13c}$$

$$N_{Re}^F = d_P^F G_m^F/\mu^F \tag{13d}$$

where P^F is the feed-side pressure (bar), P_0^F the inlet feed-side pressure, μ^F the viscosity (Pa·s), d_P^F the particle diameter in the feed side (m), $G_m^F = \rho_F^F u^F$ the superficial mass flow velocity in the feed side (kg/m^2·s), ρ_F^F the density of the fluid (kg/m^3), and g_c the gravity conversion factor equal to 1 in SI units.

Because the SiC membranes do not show substantial CO_2 permeation,[33] we assume that no adsorbent or catalyst is present in the permeate side. For the permeate side, the following equation is, therefore, utilized:

$$\frac{\partial C_j^P}{\partial t} + k\frac{\partial n_j^P}{\partial V} = \alpha_m k U_j(P_j^F - P_j^P) + (A^F)^2\frac{\partial}{\partial V}\left(D_L^P\frac{\partial C_j^P}{\partial V}\right); \quad j = 1, 2, ..., n \tag{14}$$

where $k = A^F/A^P$, with A^P being the cross-sectional area on the permeate side (m^2), and D_L^P (m^2/s) is the axial Taylor–Aris dispersion coefficient on the permeate side[36] for empty tubes given as:

$$D_L^P = D_m^P + \frac{(u^P)^2(d_t^P)^2}{192 D_m^P} \tag{15}$$

where D_m^P is the molecular diffusivity (m^2/s), u^P is the velocity at the permeate side (m/s), and d_t^P is the membrane inside diameter (m). In the simulations, the conditions prevailing in the permeate side at the start of step iv are those prevailing at steady state during step iii. In addition, during step iv the following conditions prevail in the permeate side:

$$\text{at } V = 0; \qquad \frac{\partial x_j^P}{\partial V} = -\frac{u_0^P(x_{j0}^P - x_j^P)}{A^F D_L^P} \tag{16a}$$

$$\text{at } V = V_R; \qquad \frac{\partial x_j^P}{\partial V} = 0 \tag{16b}$$

where x_j^P is the mole fraction, x_{j0}^P the inlet mole fraction for species j on the permeate side, and u_0^P the superficial flow velocity (m/s) at the inlet. Because no adsorbent or catalyst is present in the permeate side, we ignore any potential pressure drops.

The reactor conversion (based on methane, which is typically the limiting reagent) is defined by the following equation:

$$X_{CH_4} = \frac{n^F_{CH_4,0} - (n^F_{CH_4,ex} + n^P_{CH_4,ex})}{n^F_{CH_4,0}} \quad (17)$$

where $n^F_{CH_4,0}$ is the inlet molar flow rate of CH_4 and $n^F_{CH_4,ex}$ and $n^P_{CH_4,ex}$ are the methane molar flow rates at the exit of the reactor feed and permeate sides correspondingly (mol/s). The yield of product hydrogen, defined as the fraction of moles of methane fed into the reactor that have reacted to produce hydrogen, is given by the following equation:

$$Y_{H_2} = \frac{1}{4}\frac{(n^F_{H_2,ex} - n^F_{H_2,0}) + (n^P_{H_2,ex} - n^P_{H_2,0})}{n^F_{CH_4,0}} \quad (18)$$

where $n^F_{H_2,ex}$ and $n^P_{H_2,ex}$ are the hydrogen molar flow rates at the exit of respectively the reactor feed and permeate sides and $n^F_{H_2,0}$ and $n^P_{H_2,0}$ the H_2 molar flow rates potentially present at the inlet of the reactor feed and permeate sides (mol/s). $Y_{H_2} = 1$ when all of the methane has reacted completely to produce CO_2 and H_2.

Equations 6−18 can be written in dimensionless form by defining the following variables and groups:

$$\tau_\alpha = (k_a)^{-1};\quad \tau_F = \frac{\epsilon^F V_R}{A^F u_0^F};\quad \gamma = \frac{\tau_F}{\tau_\alpha};\quad \eta = \frac{V}{V_R};\quad u^F = \frac{Q^F}{A^F};$$

$$u_0^F = \frac{Q_0^F}{A^F};\quad \xi^F = \frac{u^F}{u_0^F};\quad \xi^P = \frac{u^P}{u_0^P};\quad \Psi^F = \frac{P^F}{P_0^F};\quad \Psi^P = \frac{P^P}{P_0^P};$$

$$\omega = \frac{P_0^P}{P_0^F};\quad \alpha_j = \frac{MW_j}{MW_{H_2}};\quad x_j^F = \frac{P_j^F}{P^F};\quad x_j^P = \frac{P_j^P}{P^P};\quad \tau = k_a t;$$

$$\delta_j = \frac{U_j}{U_{H_2}};\quad K'_{eq1} = \frac{K_{eq1}}{(P_0^F)^2};\quad K'_{CO} = K_{CO}P_0^F;$$

$$K'_{H_2} = K_{H_2}P_0^F;\quad \beta_{CO_2} = b_{CO_2}P_0^F;$$

$$Da = \frac{\beta_c(1-\epsilon_b^F)\rho_c k_1(T_0)\, V_R RT}{A^F u_0^F (P_0^F)^{1.5}};\quad Pe = \frac{A^F u_0^F}{U_{H_2} V_R \alpha_m RT};$$

$$\Theta^F = \frac{\epsilon_b^F A^F D_L^F}{u_0^F V_R};\quad \Theta^P = \frac{A^F D_L^P}{u_0^P V_R};$$

$$Ha = \frac{(1-\beta_c)(1-\epsilon_b^F)V_R\rho_a k_a RT m_{CO_2}}{A^F u_0^F P_0^F};\quad \Lambda = \frac{Ha}{Da};$$

$$\Omega = (Da)(Pe);\quad \Xi = 10^{-6} f^F \frac{(u_0^F)^2 MW_{H_2} V_R}{A^F g_c d_p^F RT};$$

$$\lambda = \frac{A^P u_0^P}{A^F u_0^F};\quad \theta^F_{seq} = \frac{C^F_{seq}}{m_{CO_2}};\quad \theta^F_s = \frac{C^F_s}{m_{CO_2}}$$

The dimensionless equations equivalent to eqs 7−18 are

$$\gamma\frac{\partial x_j^F}{\partial \tau} = -\left(\xi^F\frac{\partial x_j^F}{\partial \eta} + x_j^F\frac{\partial \xi^F}{\partial \eta} + \frac{x_j^F \xi^F}{\Psi^F}\frac{\partial \Psi^F}{\partial \eta}\right) - \frac{Da\delta_j}{\Omega}\left(x_j^F - x_j^P\omega\frac{\Psi^P}{\Psi^F}\right) + Da\frac{1}{\Psi^F}R'^j_F - Da\Lambda\frac{1}{\Psi^F}G'^j_F + \Theta^F\frac{\partial^2 x_j^F}{\partial \eta^2} + 2\Theta^F\frac{1}{\Psi^F}\left(\frac{\partial x_j^F}{\partial \eta}\right)\left(\frac{\partial \Psi^F}{\partial \eta}\right);$$
$$j = 1, 2, ..., n-1 \quad (19)$$

$$\frac{\partial \xi^F}{\partial \eta} = -\frac{\xi^F}{\Psi^F}\frac{\partial \Psi^F}{\partial \eta} - \frac{Da}{\Omega}\sum_j \delta_j\left(x_j^F - x_j^P\omega\frac{\Psi^P}{\Psi^F}\right) + Da\frac{1}{\Psi^F}\sum_j R'^j_F - \Lambda Da\frac{1}{\Psi^F}G'^F_{CO_2} \quad (20)$$

$$\frac{\gamma}{\epsilon^F\lambda k}\frac{\partial x_j^P}{\partial \tau} = -\left(\xi^P\frac{\partial x_j^P}{\partial \eta} + x_j^P\frac{\partial \xi^P}{\partial \eta} + \frac{x_j^P\xi^P}{\Psi^P}\frac{\partial \Psi^P}{\partial \eta}\right) + \frac{Da\delta_j}{\lambda\Omega}\left(x_j^F\frac{\Psi^F}{\omega\Psi^P} - x_j^P\right) + \Theta^P\frac{\partial^2 x_j^P}{\partial \eta^2} + 2\Theta^P\frac{1}{\Psi^P}\left(\frac{\partial x_j^P}{\partial \eta}\right)\left(\frac{\partial \Psi^P}{\partial \eta}\right);$$
$$j = 1, 2, ..., n-1 \quad (21)$$

$$\frac{\partial \xi^P}{\partial \eta} = -\frac{\xi^P}{\Psi^P}\frac{\partial \Psi^P}{\partial \eta} + \frac{Da}{\lambda\Omega}\sum_j \delta_j\left(x_j^F\frac{\Psi^F}{\omega\Psi^P} - x_j^P\right) \quad (22)$$

$$\partial\Psi^F/\partial\eta = -\Xi(\xi^F)^2\Psi^F\sum x_j^F\alpha_j \quad (23)$$

$$d\theta^F_s/d\tau = \theta^F_{seq} - \theta^F_s \quad (24)$$

$$X_{CH_4} = \frac{x^F_{CH_4,0} - (x^F_{CH_4}\Psi^F\xi^F)_{ex} + (x^P_{CH_4}\lambda\Psi^P\omega\xi^P)_{ex}}{x^F_{CH_4,0}} \quad (25)$$

$$Y_{H_2} = \frac{1}{4}\frac{(x^F_{H_2}\Psi^F\xi^F)_{ex} - x^F_{H_2,0} + (x^P_{H_2}\lambda\Psi^P\omega\xi^P)_{ex} - x^P_{H_2,0}\lambda\omega}{x^F_{CH_4,0}} \quad (26)$$

where in dimensionless form:

$$G'^F_{CO_2} = (\theta^F_{seq} - \theta^F_s) \quad (27)$$

$$\theta^F_{seq} = \frac{\beta_{CO_2}x^F_{CO_2}\Psi^F}{1 + \beta_{CO_2}x^F_{CO_2}\Psi^F} \quad (28)$$

and R'_j are dimensionless forms of R_j, which are described by eqs 1−5, with the dimensionless forms of the rates $r'_1 - r'_3$ shown in Table 3. Equations 20 and 22 that express the dimensionless velocity distributions are obtained by overall mass balances in the feed and permeate sides. In the absence of substantial pressure drop in the permeate side in eq 21, $\Psi^P = 1$ and $\partial\Psi^P/\partial\eta = 0$. The initial conditions at the start of the adsorption/reaction step are those prevailing during step

Table 3. Dimensionless Rate Expressions for the Methane−Steam-Reforming Reaction[a]

i	reaction	rate expression
1	$CH_4 + H_2O \leftrightarrow CO + 3H_2$	$r'_1 = (1/\mathrm{DEN}^2 x_{H_2}^{2.5}\Psi^{0.5})[x_{CH_4}x_{H_2O} - (P_0\Psi)^2(x_{H_2}^3 x_{CO}/K_{eq1})]$
2	$CO + H_2O \leftrightarrow CO_2 + H_2$	$r'_2 = (k_2/k_1)[(P_0^F)^{1.5}\Psi/\mathrm{DEN}^2 x_{H_2}][x_{CO}x_{H_2O} - x_{H_2}x_{CO_2}/K_{eq2}]$
3	$CH_4 + 2H_2O \leftrightarrow CO_2 + 4H_2$	$r'_3 = (k_3/k_1)[1/\mathrm{DEN}^2 x_{H_2}^{3.5}\Psi^{0.5}][x_{CH_4}x_{H_2O}^2 - (P_0\Psi)^2(x_{H_2}^4 x_{CO_2}/K_{eq3})]$

[a] $\mathrm{DEN} = 1 + K'_{CO}\Psi^F x_{CO} + K'_{H_2}\Psi^F x_{H_2} + K'_{CH_4} + K_{H_2O}(x_{H_2O}/x_{H_2})$.

3 previously described. In addition, the following boundary conditions also apply:

for $\tau > 0$, at $\eta = 0$:

$$\Psi^F = 1, \quad \Psi^P = 1 \tag{29a}$$

$$\xi^F = 1; \quad \xi^P = 1 \tag{29b}$$

$$\frac{\partial x_j^F}{\partial \eta} = -\frac{1}{\Theta^F}(x_{j0}^F - x_j^F); \quad j = 1, 2, ..., n \tag{29c}$$

$$\frac{\partial x_j^P}{\partial \eta} = -\frac{1}{\Theta^P}(x_{j0}^P - x_j^P); \quad j = 1, 2, ..., n \tag{29d}$$

for $\tau > 0$, at $\eta = 1$:

$$\frac{\partial x_j^F}{\partial \eta} = 0 \tag{30a}$$

$$\frac{\partial x_j^P}{\partial \eta} = 0 \tag{30b}$$

where $s = \sum n_{j0}^P / \sum n_{j0}^F = \lambda\omega(\sum x_{j0}^P / \sum x_{j0}^F)$ is the sweep ratio for the MR.

The system of coupled nonlinear partial differential equations (19)−(24) and accompanying boundary conditions has been solved in MATLAB using the method of lines.[37,38] The system of partial differential equations was converted to a set of ordinary differential equations by discretizing the spatial derivative in the η direction using a five-point-biased upwind finite-difference scheme to approximate the convective term. A fourth-order central-difference scheme has been used to approximate the diffusive term. For finite differences, the reactor volume was divided into n sections with $n + 1$ nodes. The initial value ordinary differential equations and other explicit algebraic equations at a time τ were simultaneously solved using ode45.m, a MATLAB built-in solver for initial value problems for ordinary differential equations.

3. Results and Discussion

We report here the behavior of the HAMR and AR at two temperatures (400 and 480 °C) for which experimental data for the adsorption rates were previously reported by Ding and Alpay.[22,27] The Xu and Froment steam-reforming kinetics were used previously[16−20,22,27,29−32] at temperatures as low as 450 °C. Previously, our group[39] also showed the same kinetics to be consistent with experimental data generated with a commercial Ni-based catalyst at temperatures as low as 450 °C. The applicability of these kinetics at temperatures lower than 450 °C still remains to be proven, however.

Figure 2 shows the hydrogen yield attained by both the ARs and HAMRs as a function of dimensionless time τ for different values of $W_c/n_{CH_4,0}^F$ (W_c is the total weight of the catalyst). The reactor temperature is 480 °C, and a $CH_4/H_2O/H_2$ feed ratio of 1:3:0.1 is utilized. Steam is used as the sweep gas. The adsorption rates and

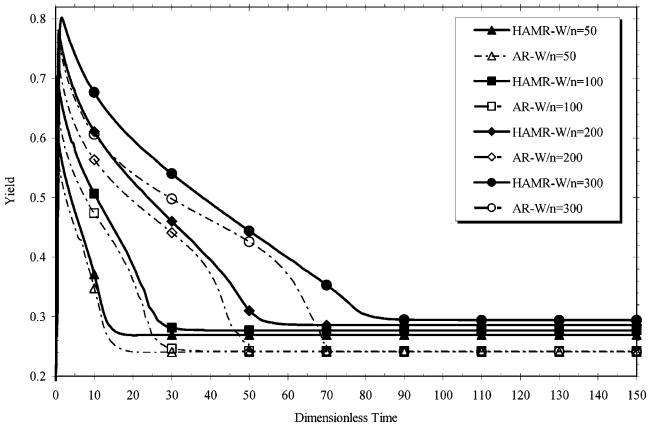

Figure 2. H_2 yield for the HAMR and AR systems for different $W_c/n_{CH_4,0}^F$.

Table 4. Parameter Values Used in Simulations

parameter	value	dimension
b_{CO_2}	1.93×10^1	bar^{-1}
d_p^F	1.00×10^{-3}	m
Da	2.62	− (base case)
Ha	7.01	− (base case)
k	2.00	−
m_{CO_2}	5.80×10^{-1}	mol/kg
Pe	5.80×10^{-1}	− (base case)
P_0^F	3.00	bar
P_0^P	2.00	bar
s	1.00×10^{-1}	− (base case)
T	4.80×10^2	°C (base case)
u_0^F	4.06×10^{-2}	m/s
u_0^P	1.22×10^{-2}	m/s
U_{H_2}	1.54×10^{-2}	$\mathrm{mol/m^2 \cdot s \cdot bar}$
V_R/A^F	2.54×10^{-1}	m
α_m	2.86×10^2	$\mathrm{m^2/m^3}$
β_c	5.00×10^{-1}	−
β_{CO_2}	1.93×10^1	−
γ	2.80×10^{-1}	−
δ_1	1.00	−
δ_2	2.80×10^{-2}	−
δ_3	2.10×10^{-1}	−
δ_4	3.55×10^{-1}	−
ϵ^F	4.00×10^{-1}	−
Λ	2.67	−
λ	5.00×10^{-1}	−
μ^F	2.87×10^{-5}	Pa·s
τ_F	2.50	−
τ_α	1.00×10^1	−
Ω	1.54	−
ω	6.60×10^{-1}	−

constants are taken directly from Ding and Alpay,[27] the reaction rate constants are from Xu and Froment,[8] and the membrane permeances are the experimental values measured with one of our own SiC membranes. Table 4 lists the values of all of the other parameters utilized (λ, β_c, ω, V_R/A^F, s, P_0^F, etc.). Initially, the hydrogen yield for both reactors reaches high values, but it declines as the adsorbent becomes saturated and levels off at the corresponding values for the conventional membrane (in the case of HAMR) or the plug-flow reactor (in the case of AR). The HAMR performs significantly better than

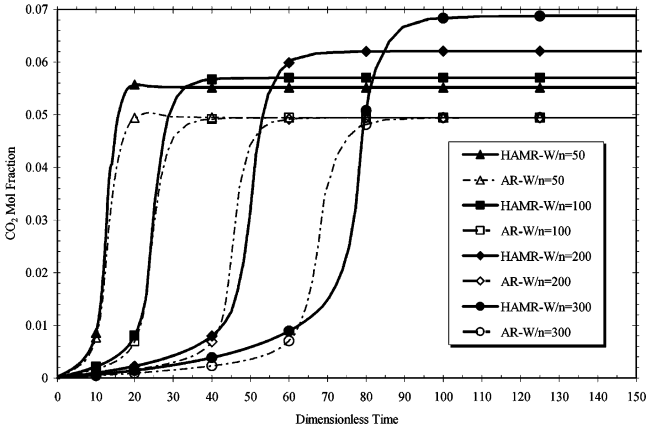

Figure 3. CO_2 concentration (wet basis) profiles at the reactor outlet for the AR and HAMR systems at different $W_c/n^F_{CH_4,0}$.

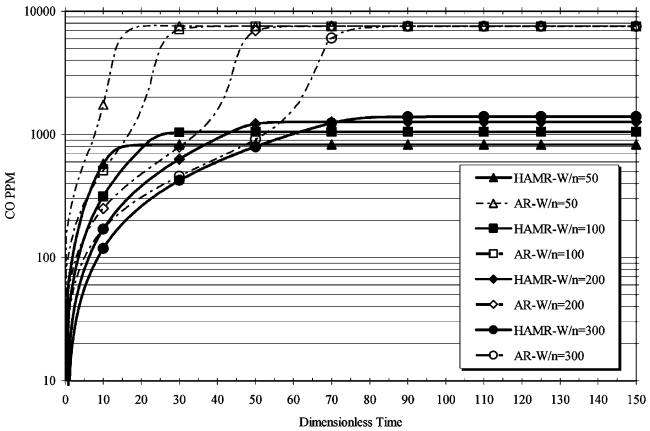

Figure 4. CO concentration (wet basis, in ppm) profiles in the HAMR permeate-side exit and AR exit for different $W_c/n^F_{CH_4,0}$.

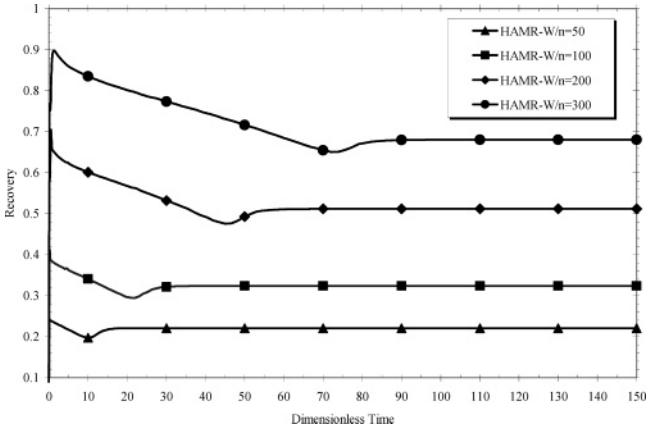

Figure 5. Hydrogen recovery for the HAMR system at different $W_c/n^F_{CH_4,0}$.

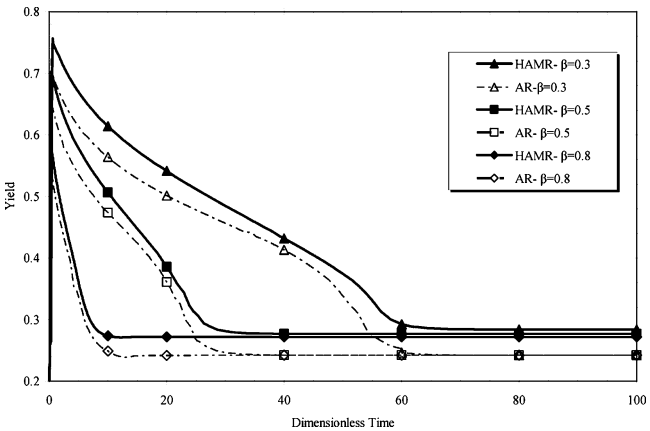

Figure 6. Effect of β_c on the hydrogen yields for both the HAMR and AR systems.

the AR. For the conditions in Figure 2, the catalyst is sufficiently active that the plug-flow reactor yields (the AR yields level off at these values) approach equilibrium (~24.2% under the prevailing conditions) for all of the four $W_c/n^F_{CH_4,0}$ values utilized. On the other hand, the yields for the AR and HAMR systems (prior to the adsorbent saturation) and the MR yields (the HAMR yields level off at these yields) strongly depend on $W_c/n^F_{CH_4,0}$, increasing as $W_c/n^F_{CH_4,0}$ increases, as expected.

Figure 3 shows the CO_2 feed-side exit concentration (wet basis) profiles for the HAMR and AR. Low concentrations are observed while the adsorbent remains unsaturated; the concentrations sharply increase, however, after the adsorbent is saturated. Figure 4 shows the CO concentration (wet basis) profiles in the permeate-side exit of the HAMR, together with the corresponding exit concentration values for the AR. Clear from Figure 4 is the advantage that the HAMR system provides in terms of reduced CO concentrations in the hydrogen product over the AR system, in addition to improved hydrogen yields.

A potential disadvantage of the HAMR system, when compared to the AR system, is that only a fraction of the hydrogen product ends up in the permeate stream, while the rest remains mixed with the unreacted CH_4 and the CO and CO_2 products in the feed-side stream. Figure 5 shows the hydrogen recovery rate, which is defined as the fraction of the total hydrogen that is produced in the HAMR that ends up in the permeate stream, that is, the hydrogen molar flow in the permeate side divided by the total hydrogen molar flow (feed side plus permeate side). The increase in the hydrogen recovery, shown in Figure 5, coincides with the CO_2 breakthrough, which results in a sharp decrease in the molar flow of hydrogen in the feed side (less hydrogen is produced there because the adsorbent no longer removes the CO_2 produced). Because the total hydrogen molar flow rate also declines, hydrogen recovery increases and finally levels off at the corresponding steady-state (AR or MR) levels. The hydrogen recovery is, of course, a strong function of the membrane permeation characteristics and the other operating conditions in the reactor, increasing with increasing membrane permeance and feed-side pressure. Furthermore, one must also take into account, when comparing both reactors, that even for the AR system one must eventually separate the hydrogen out of the exit stream and that similar hydrogen losses are likely to occur.

Figure 6 shows the effect of β_c (the fraction of reactor volume occupied by catalyst) on the hydrogen yields, while keeping the total volume occupied by the solids and the $W_c/n^F_{CH_4,0}$ constant. Decreasing β_c (i.e., increasing the fraction of sorbent present), while maintaining $W_c/n^F_{CH_4,0}$ constant, has a significant beneficial effect on the hydrogen yield and also on the product purity for both the HAMR and AR systems (see Figure 7 for the CO content of the hydrogen product).

The effect of using an adsorbent with improved characteristics is shown in Figure 8. The hydrogen yields for the HAMR and AR systems are compared for three values of Λ, one corresponding to the adsorbent of Ding and Alpay[27] (for the reactor temperature and

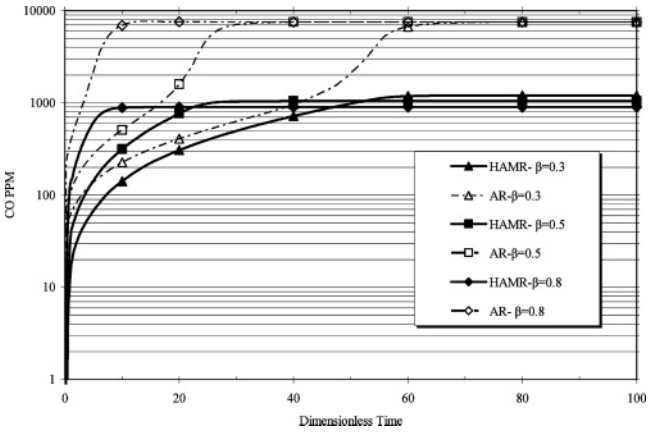

Figure 7. Effect of β_c on the CO exit concentration (wet basis, in ppm) for the HAMR (permeate) and AR systems.

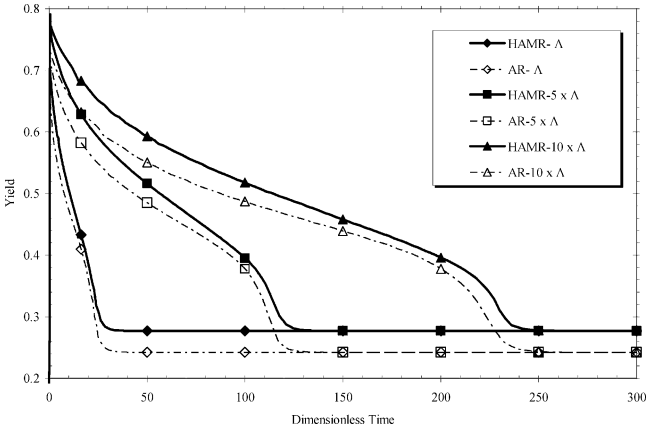

Figure 8. Effect of Λ on the hydrogen yield.

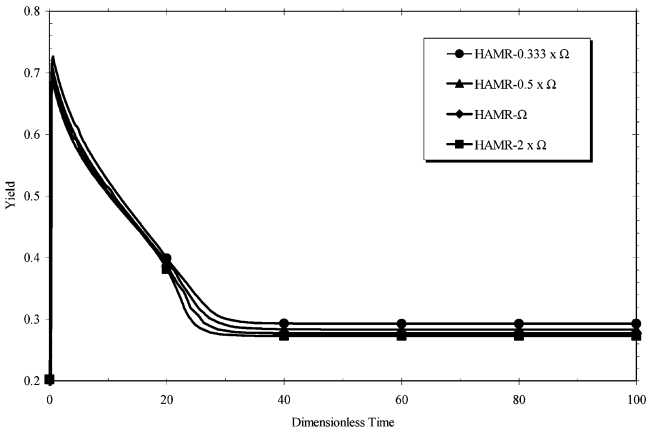

Figure 9. Effect of Ω on the hydrogen yield.

pressure conditions utilized, this corresponds to Λ = 2.67) and two other cases with corresponding Λ values 5 and 10 times larger. A more effective adsorbent significantly expands the "time window" of operation for both the AR and HAMR systems before regeneration must commence. It also significantly increases the hydrogen yields attained.

The effect of membrane transport characteristics is shown in Figure 9, where the reactor yields corresponding to four different membranes (i.e., four different values of Ω) are shown. For the SiC membrane used in the simulations, Ω = 1.54. The other three membranes have Ω values that are 0.333, 0.5, and 2 times the base Ω value (because Ω is inversely proportional to permeance, these Ω values correspond to permeances that are 3, 2, and 0.5 times that of the base case corresponding to Ω = 1.54). The HAMR system hydrogen yields do benefit from increased hydrogen permeance, but the effect saturates beyond a certain value. Figure 10 shows the effect that Ω has on hydrogen recovery. As expected, increasing the hydrogen permeance has a very beneficial effect on hydrogen recovery, with very high hydrogen recoveries (~87%) attained for 0.333 times the base case Ω. Figure 11 shows the effect of the sweep ratio on the hydrogen yield of the HAMR system. Increasing the sweep ratio improves the reactor performance; however, the effect saturates quickly, as shown in Figure 11.

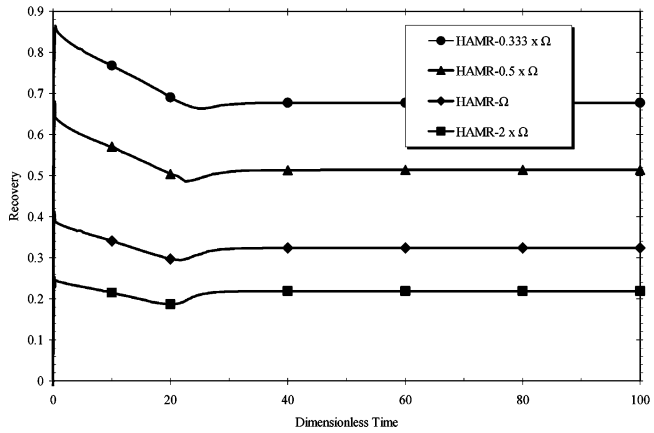

Figure 10. Effect of Ω on the hydrogen recovery.

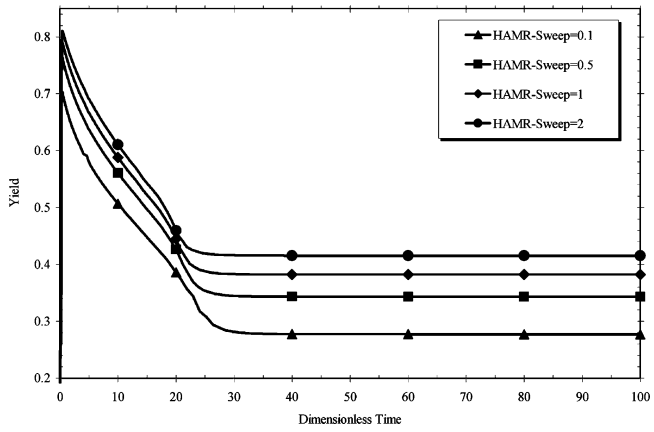

Figure 11. Effect of the sweep ratio on the hydrogen yield.

Figures 12 and 13 show the behavior of the two systems at 400 °C. Figure 12 shows the hydrogen yield, while Figure 13 presents the time-averaged CO (wet basis, in ppm) content for both the HAMR and AR systems. The average CO purity, $\langle y_{CO} \rangle$, at the given operating time t_1 is calculated by:

$$\langle y_{CO} \rangle = \frac{\int_0^{t_1} \left(\frac{Pu^P y_{CO}}{RT} \right)_{outlet} dt}{\int_0^{t_1} \left(\frac{Pu^P}{RT} \right)_{outlet} dt} \quad \text{for HAMR;}$$

$$\langle y_{CO} \rangle = \frac{\int_0^{t_1} \left(\frac{Puy_{CO}}{RT} \right)_{outlet} dt}{\int_0^{t_1} \left(\frac{Pu}{RT} \right)_{outlet} dt} \quad \text{for AR}$$

The conditions in the figure are such that for a good

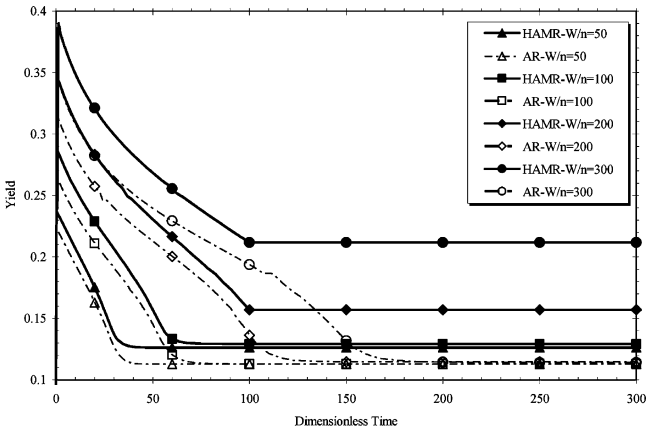

Figure 12. Hydrogen yield at 400 °C.

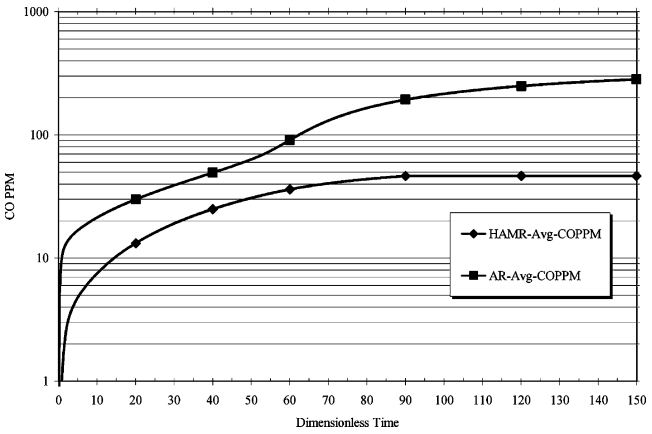

Figure 13. Time-averaged CO concentration (wet basis, in ppm) at 400 °C for the HAMR and AR systems.

fraction of the adsorption/reaction cycle for the HAMR system the CO content in the hydrogen product stays below 50 ppm (140 ppm on a dry basis).

4. Conclusions

We have investigated a novel reactor system, termed the HAMR, for hydrogen production through methane–steam reforming. The HAMR combines the reaction and membrane separation steps with adsorption on the membrane feed or permeate sides. The HAMR system is of potential interest to pure hydrogen production for proton exchange membrane (PEM) fuel cells for various mobile and stationary applications. The reactor characteristics have been investigated for a range of temperature, pressure, and other experimental conditions relevant to the aforementioned applications and compared with the behavior of the traditional packed-bed reactor, the conventional MR, and an AR. The HAMR outperforms all of the other more conventional reactor systems. It exhibits enhanced methane conversion, hydrogen yield, and product purity and shows good promise for reducing the hostile operating conditions of conventional methane–steam reformers and for meeting the product purity requirements for PEM operation. The performance of the HAMR system depends on the various operating parameters, including the reactor space time, the temperature, and the membrane and adsorbent properties. Use of more effective adsorbents results, for example, in increased yields and longer operational windows. More highly permeable membranes also increase the reactor yield but, more importantly, also increase the hydrogen recovery ratio. One of the key advantages of the HAMR system over the corresponding AR system (in addition to improvements in yield) is its ability to deliver a product with a significantly lower CO content through the use of membranes, which preferentially allow the permeation of the hydrogen while excluding CO and other reactants and products. This may be the primary reason for adopting such reactors for fuel-cell application, where a CO-free product is at a premium.

The downside of the HAMR system is, similar to that for the ARs, in that they require regeneration of the spent adsorbent and, for continuous operation, they may require a dual reactor system, where one of the reactors is in operation while the other reactor is being regenerated. In future publications, we will provide experimental validation of the HAMR system and extend the model to incorporate adsorbent regeneration.

Acknowledgment

This work was financially supported by NASA and the U.S. Department of Energy.

Nomenclature

A^F = cross-sectional area for the reactor feed side (m^2)
A^P = cross-sectional area for the reactor permeate side (m^2)
b_{CO_2} = Langmuir model adsorption equilibrium constant for CO_2 (bar^{-1})
C_j^F = gas-phase concentration of species j in the feed side ($kmol/m^3$)
C_j^P = gas-phase concentration of species j in the permeate side ($kmol/m^3$)
C_s = solid-phase concentration of CO_2 (mol/kg)
C_{seq} = equilibrium solid-phase concentration of CO_2 (mol/kg)
Da = Damkohler number
D_L^F = axial dispersion coefficient in the feed side (m^2/s)
D_L^P = axial dispersion coefficient in the permeate side (m^2/s)
D_m^F = molecular diffusivity in the feed side (m^2/s)
D_m^P = molecular diffusivity in the permeate side (m^2/s)
d_t^p = membrane inside diameter (m)
d_p^F = particle diameter in the feed side (m)
f^F = friction factor
F_j = molar flux ($mol/m^2 \cdot s$)
g_c = gravity conversion factor
G_m^F = superficial mass flow velocity in the feed side ($kg/m^2 \cdot s$)
$G_j'^F$ = dimensionless adsorption rate for species j
G_j^F = adsorption rate for species j ($mol/kg \cdot s$)
Ha = Hatta number
$k = A^F/A^P$
k_a = linear driving force mass-transfer coefficient (s^{-1})
K_j = adsorption equilibrium constant for CH_4, CO, and H_2 (bar^{-1})
K_{H_2O} = dissociative adsorption constant of water
K'_{CO} = dimensionless kinetic parameter
K_{eq1}, K_{eq3} = equilibrium constant of reactions I and III in Table 1 (bar^2)
K_{eq2} = equilibrium constant of reaction I in Table 1
m_{CO_2} = Langmuir model total adsorbent capacity constant for CO_2 (mol/kg)
MW_j = molecular weight of species j
N_{Re}^F = Reynolds number for the feed side

J

n_{j0}^{F} = inlet molar flow rate for the feed side (mol/s)
n_{j0}^{P} = inlet molar flow rate for the permeate side (mol/s)
n_j^{F} = molar flow rate for component j in the feed side (mol/s)
n_j^{P} = molar flow rate for component j in the permeate side (mol/s)
$n_{i,ex}^{F}$ = molar flow rates at the exit of the reactor for component i in the feed side (mol/s)
$n_{i,ex}^{P}$ = molar flow rates at the exit of the reactor for component i in the permeate side (mol/s)
P_0^{F} = inlet feed side pressure (bar)
Pe = Peclet number
P^{F} = feed side pressure (bar)
P_j^{F} = partial pressure of component j in the membrane feed side (bar)
P_j^{P} = partial pressure of component j in the membrane permeate side (bar)
Q_0^{F} = volumetric flow rate (m^3/s)
R = ideal gas constant (m^3·bar/mol·K)
r_i = rate of reaction for the ith equation (kmol/kg·s)
r_i' = dimensionless rate of reaction for the ith equation
R_j = reaction rate expression for species j (kmol/kg·s)
R_j' = dimensionless reaction rate expression for species j
s = sweep ratio
t = time (s)
T = absolute temperature (K)
T_0 = reference temperature (K)
u_0^{F} = superficial flow velocity at the inlet on the feed side (m/s)
u_0^{P} = superficial flow velocity at the inlet on the permeate side (m/s)
u^{F} = superficial flow velocity on the feed side (m/s)
u^{P} = superficial flow velocity on the permeate side (m/s)
U_j = membrane permeance for component j (mol/m^2·bar·s)
V = reactor volume (m^3)
V_R = total reactor volume (m^3)
W_c = catalyst weight (kg)
X_{CH_4} = methane conversion
x_{j0}^{F} = inlet mole fraction for species j in the feed side
x_{j0}^{P} = inlet mole fraction for species j in the permeate side
x_j^{F} = mole fraction for species j in the feed side
x_j^{P} = mole fraction for species j in the permeate side
y_j = mole fraction of component j
Y_{H_2} = hydrogen yield

Subscripts

0 = entrance condition
ads = adsorbent condition
eq = equilibrium
ex = exit
j = chemical species

Superscripts

F = feed side
P = permeate side

Greek Letters

α_m = membrane area per feed-side reactor volume (m^2/m^3)
$\alpha_j = MW_j/MW_{H_2}$
β_c = fraction of the reactor volume occupied by catalysts
$\beta_{CO_2} = b_{CO_2}P_0^{F}$
$\gamma = \tau_F/\tau_\alpha$
ΔH_a = heat of adsorption (kJ/mol)
δ_j = separation factor
ϵ^{F} = total feed-side bed porosity
ϵ_b^{F} = bed porosity in the feed side
$\xi^{F} = u^{F}/u_0^{F}$
$\xi^{P} = u^{P}/u_0^{P}$
$\eta = V/V_R$
$\Theta^{F} = \epsilon_b^{F}A^{F}D_L^{F}/u_0^{F}V_R$
$\Theta^{P} = A^{F}D_L^{P}/u_0^{P}V_R$
$\theta_s^{F} = C_s^{F}/m_{CO_2}$
$\theta_{seq}^{F} = C_{seq}^{F}/m_{CO_2}$
$\Lambda = Ha/Da$
$\lambda = A^{P}u_0^{P}/A^{F}u_0^{F}$
μ^{F} = viscosity (Pa·s)
$\Xi = 10^{-6}f^{F}[(u_0^{F})^2 MW_{H_2}V_R/A^{F}g_c d_p^{F}RT]$
ρ_a = adsorbent density (kg/m^3)
ρ_c = catalyst density (kg/m^3)
ρ_F^{F} = fluid density (kg/m^3)
$\tau = k_a t$
$\tau_F = \epsilon^{F}V_R/A^{F}u_0^{F}$
$\tau_\alpha = (k_a)^{-1}$
$\Psi^{F} = P^{F}/P_0^{F}$
$\Psi^{P} = P^{P}/P_0^{P}$
$\Omega = (Da)(Pe)$
$\omega = P_0^{P}/P_0^{F}$

Literature Cited

(1) Park, B. Models and Experiments with Pervaporation Membrane Reactors Integrated with a Water Removal Adsorbent System. Ph.D. Thesis, University of Southern California, Los Angeles, CA, 2001.

(2) Park, B.; Tsotsis, T. T. Models and Experiments with Pervaporation Membrane Reactors Integrated with an Adsorbent System. *Chem. Eng. Proc.* **2004**, *43*, 1171.

(3) Choi, Y.; Stenger, H. G. Water Gas Shift Reaction Kinetics and Reactor Modeling for Fuel Cell Grade Hydrogen. *J. Power Sources* **2003**, *124*, 432.

(4) Darwish, N. A.; Hilal, N.; Versteeg, G.; Heesink, B. Feasibility of the Direct Generation of Hydrogen for Fuel-cell-powered Vehicles by on-board Steam Reforming of Naphtha. *Fuel* **2003**, *83*, 409.

(5) Liu, Z.; Roh, H.; Park, S. Hydrogen Production for Fuel Cells through Methane Reforming at Low Temperatures. *J. Power Sources* **2002**, *111*, 83.

(6) Semelsberger, T. A.; Brown, L. F.; Borup, R. L.; Inbody, M. A. Equilibrium Products from Autothermal Processes for Generating Hydrogen-rich Fuel-cell Feeds. *Int. J. Hydrogen Energy* **2004**, *29*, 1047.

(7) Elnashaie, S. S. E. H.; Adris, A.; Al-Ubaid, A. S.; Soliman, M. A. On the Non-monotonic Behavior of Methane−steam Reforming Kinetics. *Chem. Eng. Sci.* **1990**, *45*, 491.

(8) Xu, J.; Froment, G. F. Methane Steam Reforming, Methanation and Water-gas Shift: I. Intrinsic Kinetics. *AIChE J.* **1989**, *35*, 88.

(9) Han, C.; Harrison, D. P. Simultaneous Shift Reaction and Carbon Dioxide Separation for the Direct Production of Hydrogen. *Chem. Eng. Sci.* **1994**, *49*, 5875.

(10) Hwang, S. Inorganic Membranes and Membrane Reactors. *Korean J. Chem. Eng.* **2001**, *18*, 775.

(11) Lim, S. Y.; Park, B.; Hung, F.; Sahimi, M.; Tsotsis, T. T. Design Issues of Pervaporation Membrane Reactors for Esterification. *Chem. Eng. Sci.* **2002**, *57*, 4933.

(12) Park, B.; Ravi-Kumar, V. S.; Tsotsis, T. T. Models and Simulation of Liquid-phase Membrane Reactors. *Ind. Eng. Chem. Res.* **1998**, *37*, 1276.

(13) Nam, S. W.; Yoon, S. P.; Ha, H. Y.; Hong, S.; Maganyuk, A. P. Methane Steam Reforming in a Pd−Ru Membrane Reactor. *Korean J. Chem. Eng.* **2000**, *17*, 288.

(14) Saracco, G.; Specchia, V. Catalytic Inorganic-membrane Reactors: Present Experience and Future Opportunities. *Catal. Rev.−Sci. Eng.* **1994**, *36*, 305.

(15) Sanchez, J.; Tsotsis, T. T. *Catalytic Membranes and Membrane Reactors*; Wiley-VCH: Weinheim, Germany, 2002.

(16) Xiu, G. H.; Li, P.; Rodrigues, A. E. Subsection-controlling Strategy for Improving Sorption-enhanced Reaction Process. *Chem. Eng. Res. Des.* **2004**, *82*, 192.

(17) Xiu, G.; Li, P.; Rodrigues, A. E. Adsorption-enhanced Steam−methane Reforming with Intraparticle-diffusion Limitations. *Chem. Eng. J. (Amsterdam, Neth.)* **2003**, *95*, 83.

(18) Xiu, G.; Li, P.; Rodrigues, A. E. New Generalized Strategy for Improving Sorption-enhanced Reaction Process. *Chem. Eng. Sci.* **2003**, *58*, 3425.

(19) Xiu, G.; Soares, J. L.; Li, P.; Rodrigues, A. E. Simulation of Five-step One-bed Sorption-enhanced Reaction Process. *AIChE J.* **2002**, *48*, 817.

(20) Xiu, G.; Li, P.; Rodrigues, A. E. Sorption-enhanced Reaction Process with Reactive Regeneration. *Chem. Eng. Sci.* **2002**, *57*, 3893.

(21) Lee, D. K.; Baek, I. H.; Yoon, W. L. Modeling and Simulation for the Methane Steam Reforming Enhanced by in Situ CO_2 Removal Utilizing the CaO Carbonation for H_2 Production. *Chem. Eng. Sci.* **2004**, *59*, 931.

(22) Ding, Y.; Alpay, E. Adsorption-enhanced Steam−methane Reforming. *Chem. Eng. Sci.* **2000**, *55*, 3929.

(23) Ortiz, A. L.; Harrison, D. P. Hydrogen Production Using Sorption-Enhanced Reaction. *Ind. Eng. Chem. Res.* **2001**, *40*, 5102.

(24) Balasubramanian, B.; Ortiz, A. L.; Kaytakoglu, S.; Harrison, D. P. Hydrogen from Methane in a Single-step Process. *Chem. Eng. Sci.* **1999**, *54*, 3543.

(25) Waldron, W. E.; Hufton, J. R.; Sircar, S. Production of Hydrogen by Cyclic Sorption Enhanced Reaction Process. *AIChE J.* **2001**, *47*, 1477.

(26) Hufton, J. R.; Mayorga, S.; Sircar, S. Sorption-enhanced Reaction Process for Hydrogen Production. *AIChE J.* **1999**, *45*, 248.

(27) Ding, Y.; Alpay, E. Equilibria and Kinetics of CO_2 Adsorption on Hydrotalcite Adsorbent. *Chem. Eng. Sci.* **2000**, *55*, 3461.

(28) Park, B. A Hybrid Adsorbent-membrane Reactor (HAMR) System for Hydrogen Production. *Korean J. Chem. Eng.* **2004**, *21*, 782.

(29) Chen, Z.; Elnashaie, S. S. E. H. Bifurcation Behavior and Efficient Pure Hydrogen Production for Fuel Cells Using a Novel Autothermic Membrane Circulating Fluidized-Bed (CFB) Reformer: Sequential Debottlenecking and the Contribution of John Grace. *Ind. Eng. Chem. Res.* **2004**, *43*, 5449.

(30) Prasad, P.; Elnashaie, S. S. E. H. Novel Circulating Fluidized-Bed Membrane Reformer Using Carbon Dioxide Sequestration. *Ind. Eng. Chem. Res.* **2004**, *43*, 494.

(31) Prasad, P.; Elnashaie, S. S. E. H. Coupled Steam and Oxidative Reforming for Hydrogen Production in a Novel Membrane Circulating Fluidized-Bed Reformer. *Ind. Eng. Chem. Res.* **2003**, *42*, 4715.

(32) Chen, Z.; Yan, Y.; Elnashaie, S. S. E. H. Novel Circulating Fast Fluidized-bed Membrane Reformer for Efficient Production of Hydrogen from Steam Reforming of Methane. *Chem. Eng. Sci.* **2003**, *58*, 4335.

(33) Ciora, R. J.; Fayyaz, B.; Liu, P. K. T.; Suwanmethanond, V.; Mallada, R.; Sahimi, M.; Tsotsis, T. T. Preparation and Reactive Applications of Nanoporous Silicon Carbide Membranes. *Chem. Eng. Sci.* **2004**, *59*, 4957.

(34) Edwards, M. F.; Richardson, J. F. Gas Dispersion in Packed Beds. *Chem. Eng. Sci.* **1968**, *23*, 109.

(35) Karger, J.; Ruthven, D. M. *Diffusion in Zeolites and Other Microporous Solids*; Wiley Publishers: New York, 1992.

(36) Levenspiel, O. *Chemical Reaction Engineering*, 3rd ed.; Wiley: New York, 1998.

(37) Schiesser, W. E. *The Numerical Method of Lines: Integration of Partial Differential Equations*; Academic Press: San Diego, 1991.

(38) Vande Wouwer, A.; Saucez, P.; Schiesser, W. E. Simulation of Distributed Parameter Systems Using a Matlab-Based Method of Lines Toolbox: Chemical Engineering Applications. *Ind. Eng. Chem. Res.* **2004**, *43*, 3469.

(39) Vasileiadis, S. P. Catalytic Ceramic Membrane Reactors for the Methane−Steam Reforming Reaction: Experiments and Simulation. Ph.D. Thesis, University of Southern California, Los Angeles, CA, 1994.

Received for review February 18, 2005
Revised manuscript received April 6, 2005
Accepted April 8, 2005

IE050199U